A SUBROUTINE FOR THE FAST ESTIMATE OF ION CYCLOTRON HEATING EFFICIENCY IN TOKAMAK PLASMAS

M. Brambilla

IPP 5/13 February 1987

MAX-PLANCK-INSTITUT FÜR PLASMAPHYSIK

8046 GARCHING BEI MÜNCHEN

MAX-PLANCK-INSTITUT FÜR PLASMAPHYSIK

GARCHING BEI MÜNCHEN

A SUBROUTINE FOR THE FAST ESTIMATE OF ION CYCLOTRON HEATING EFFICIENCY IN TOKAMAK PLASMAS

M. Brambilla

IPP 5/13 February 1987

Die nachstehende Arbeit wurde im Rahmen des Vertrages zwischen dem Max-Planck-Institut für Plasmaphysik und der Europäischen Atomgemeinschaft über die Zusammenarbeit auf dem Gebiete der Plasmaphysik durchgeführt.

A SUBROUTINE FOR THE FAST ESTIMATE OF ION CYCLOTRON HEATING EFFICIENCY IN TOKAMAK PLASMAS

M. Brambilla

IPP 5/13

Abstract

We describe a subroutine allowing the rapid simulation of Ion Cyclotron Heating in large tokamak plasmas. It is based on analytic estimates of the wave behaviour near resonances, and on drastic but reasonable simplifications of the real geometry. Given the parameters of the plasma and of the antenna, it evaluates the radiated power spectrum, the single transit and total power absorption for each particle species, and rough power deposition profiles.

The results of the simple model have been compared with the predictions of Ray Tracing over a large range of parameters, covering the most common I.C. heating scenarios. Satisfactory agreement is almost always found; unavoidable discrepancies in details can be explained from the approximations made; they are never large for situations of practical relevance. The subroutine can thus be useful for a rapid, shot to shot analysis of experimental data, or as input for transport simulation codes. Moreover it can give enlightening although qualitative information on total (multitransit) absorption, which is difficult to obtain with more sophisticated approaches such as Ray Tracing and Full Wave codes.

1 - Introduction.

Numerical modeling of Ion Cyclotron Heating in Tokamak plasmas has rapidly progressed in recent years: Ray Tracing techniques are routinely used, and the first two-dimensional Full Waves codes have also been developed (cfr. [1] -[3], for references). Both methods however require dedicated manpower and long CPU times for the complete description of even a single case. The need for a more qualitative but substantially faster analysis is felt in at least two contexts: for a shot to shot first guide during heating experiments, and to provide the input describing h.f. heating to transport codes.

A rapid evaluation of the heating efficiency is indeed possible using analytic estimates which were developed to understand and check the results of Ray Tracing and Full Waves codes, and taking advantage of the simplifications to the real geometry which are possible in very large plasmas. A typical Ray Tracing solution for a JET case is shown in Fig. 1. This figure suggests that for plasmas of large dimensions, with the I.C. antenna placed near the equatorial plane, a reasonable one-dimensional slab model can be constructed by retaining only the horizontal variations of density, temperature and magnetic field, while neglecting the poloidal magnetic field and the curvature of wavefronts. The wave behaviour near cyclotron and ion-hybrid resonances in this geometry is described by a straightforward generalisation of the classic Budden model [4]. In this way the single transit heating efficiency can be easily obtained, both globally and separately for each charged particle species. A simple algorithm further gives the total (multitransit) absorption, taking into account also losses in the wall.

Reflection, transmission and absorption near each resonance depend critically on the parallel wavenumber, which for example determines wether mode conversion or direct cyclotron damping dominates. For this reason, it is necessary to regard the h.f. field as a superposition of toroidal eigenwaves, and in the first place to have an estimate of the power spectrum radiated by the antenna. This can be obtained by weighting the Fourier spectrum of the antenna current with an exponential factor which takes into account evanescence up to the R-cut off.

Finally, we may note that resonance layers are usually relatively narrow in the horizontal direction. Fig. 1 then also suggests that radial distribution of damping will be mainly influenced by the finite vertical width of the region illuminated by the waves. Under this assumption, a simple exercise in plane geometry allows to estimate the radial power deposition profiles.

A subroutine ICEVAL based on these drastic simplifications has been written, and is presented in this report. The equations used in ICEVAL are listed in the next section

without detailed derivation. Most of them however are so simple that none is needed; for the others, more details can be found in [5] and references therein. The input and output variables and the performances of ICEVAL are summarized in the Appendix.

In Section 3 we compare the results from ICEVAL with those obtained from a Ray Tracing code, for some of the most important heating scenarios, and over a large range of parameters. Obviously, perfect agreement under all situations cannot be expected; nevertheless the agreement is in most cases much better than qualitative. Moreover, those discrepancies which do occur can be clearly traced to the approximations made. With some understanding of the limitations of the simple model, and with systematic checks with more sofisticated Ray Tracing or Full Wave codes, we feel that ICEVAL can satisfactorily fulfill the role for which it has been developed.

2 - Modelling IC heating.

2.1 - Initialisation. The first section of ICEVAL, after checking for the consistency of the input data, evaluates the position of the cyclotron resonances of all ion species,

$$X(n,\alpha) = n \cdot R \cdot \frac{\Omega_{c\alpha}}{\omega} \qquad (n = 1,2) \tag{1}$$

where $\Omega_{c\alpha}$ is the cyclotron frequency of species α on the magnetic axis, and R the major radius of the plasma. The fundamental resonances $X(1,\alpha)$ are then sorted in order of decreasing distance from the vertical axis; for those which lie within the plasma and do not belong to the majority species, the position of the nearby ion-ion resonance and cut-off are estimated using the large density, small minority concentration approximation [5]:

$$\begin{aligned} \left(\frac{\Omega_{cm}}{\omega}\right)_{COF} &= 1 + \nu_m Z_m \left(\frac{A_M/Z_M}{A_m/Z_m} - 1\right) \\ \left(\frac{\Omega_{cm}}{\omega}\right)_{RES} &= 1 + \frac{1}{2}\nu_m Z_m \left(\frac{A_m/Z_m}{A_M/Z_M} - \frac{A_M/Z_M}{A_m/Z_m}\right) \end{aligned} \tag{2}$$

Here suffixes M, m refer to the majority and minority species, respectively; $\nu_\alpha = n_\alpha/n_e$ is the concentration of species α (concentrations are assumed to be uniform throughout the plasma).

2.2 - Model antenna spectrum. The cut-off of the partial wave with toroidal wave number n_ϕ and parallel index $n_\parallel = n_\phi/(k_o R)$ (with $n_\parallel^2 > 1$) is located at the position $\psi_{COF} = r_{COF}/a$, where

$$n_\parallel^2 = \mathcal{R}_a(1 - \psi_{COF}^2) \tag{3}$$

Here

$$\mathcal{R}_a = \frac{\omega_{pM}^2}{\Omega_{cM}^2} / \left(1 + \frac{\Omega_{cM}}{\omega}\right)\Big|_a \tag{3'}$$

is the value of the element $\mathcal{R}$ of the dielectric tensor (cfr. Eq. (10) below) on the magnetic axis, evaluated taking into account only the majority species, $\alpha = M$; the influence of the magnetic field inhomogeneity on $\mathcal{R}$ is neglected in comparison to the density dependence, assumed for simplicity to be parabolic. Thus in the first place only waves such that $|n_\parallel| < \sqrt{\mathcal{R}_a}$ are propagative in the center of the plasma. For these waves the optical thickness of the evanescence layer between the plasma edge and the cut-off can be roughly estimated to be

$$\eta_{pl} \simeq \eta_o n_\perp k_o a(1 - \sqrt{\psi_{COF}}) \tag{4}$$

where η_o is a numerical constant which depends on the density profile near the plasma edge ($\eta_o = .333$ for a parabolic profile; in practice, η_o can be adjusted to match the power spectra evaluated from a complete antenna code run). In addition, if D_{ap} is the distance between the antenna conductor and the plasma, there is a contribution to evanescence from the vacuum layer,

$$\eta_v \simeq n_\perp k_o D_{ap} \tag{5}$$

In Eqs. (4) and (5), $n_\perp = \sqrt{n_\parallel^2 - 1}$, $k_o = \omega/c$, and a is the plasma radius. The power coupled to the partial wave $n_\parallel$ is assumed to be

$$P(n_\phi) = P_o \cdot |J(n_\phi)|^2 \cdot \exp(-2(\eta_v + \eta_{pl})) \tag{6}$$

where P_o is a constant such that $\sum P(n_\phi) = P_{total}$, the total power coupled, and $J(n_\phi)$ is the Fourier transform of the current distribution in the antenna (for waves with $|n_\parallel| < 1$ the exponential factor is taken to be unity). In particular, Eq. (6) allows to estimate the range of n_ϕ values to be explored, by imposing that $\eta_v + \eta_{pl}$ should not be too large.

The Fourier amplitude $J(n_\phi)$ is easily obtained assuming the current density in the anntenna to be uniform. Two kinds of antennas are foreseen:

a) dipole antenna, having a single conductor of width w_a,

$$J(n_\phi) = J_o \frac{\sin(n_\phi w_a/2R)}{n_\phi w_a/2R} \tag{7}$$

b) quadrupole antenna, with two conductors of width w_a each, separated by a gap g and excited with a phase difference ψ,

$$J(n_\phi) = J_o \cos\left(n_\phi \frac{g+w}{2R} - \frac{\psi}{2}\right) \frac{\sin(n_\phi w_a/2R)}{n_\phi w_a/2R} \tag{8}$$

2.3 - Wave behaviour near resonances. It is shown in [5] that the behaviour of a plane wave impinging on an ion-ion resonance is essentially described by the classical Budden model with optical thickness $\eta = \eta_1 + \eta_2$, where η_1 and η_2 are the contributions of the minority ($\alpha = m$) and the majority species ($\alpha = M$), respectively. Of course η_2 is different from zero if and only if the fundamental cyclotron resonance of the minority coincides with the first harmonic resonance of the majority). If $R_o = X(1,m)$ is the position of the minority cyclotron resonance,

$$\begin{aligned} \eta_1 &= \gamma_o \frac{\pi}{4} n_F(k_o R_o) \cdot \left| \frac{(n_\parallel^2 - \mathcal{R}_o)}{(n_\parallel^2 - \mathcal{L}_o)(n_\parallel^2 - \mathcal{S}_o)} \right| \cdot \frac{\omega_{pm}^2}{\Omega_{cm}^2} \\ \eta_2 &= \gamma_o \frac{\pi}{8} n_F(k_o R_o) \cdot \left(\frac{(n_\parallel^2 - \mathcal{R}_o)}{(n_\parallel^2 - \mathcal{S}_o)} \right)^2 \cdot \frac{\omega_{pM}^2}{\Omega_{cM}^2} \frac{v_{th,M}^2}{c^2} \end{aligned} \tag{9}$$

Here

$$\mathcal{R}_o = \frac{\omega_{pM}^2}{\Omega_{cM}^2} / \left(1 + \frac{\Omega_{cM}}{\omega}\right) \qquad \mathcal{L}_o = \frac{\omega_{pM}^2}{\Omega_{cM}^2} / \left(1 - \frac{\Omega_{cM}}{\omega}\right)$$
$$\mathcal{S}_o = \frac{1}{2}(\mathcal{R}_M + \mathcal{L}_M) \tag{10}$$

are the contributions of the majority species to the cold plasma dielectric tensor elements, evaluated at $X = X(m,1)$, and

$$n_F^2 = -\frac{(n_\parallel^2 - \mathcal{R}_o) \cdot (n_\parallel^2 - \mathcal{L}_o)}{(n_\parallel^2 - \mathcal{S}_o)} \tag{11}$$

is the effective refractive index of the Fast wave (i.e. the index in the absence of resonant minority ions). Finally γ_o is a numerical factor which takes into account that the wavefronts are not strictly vertical ($\gamma_o \geq 1$, where the lower limit applies to vertical wavefronts; in practice, γ_o can be adjusted to match the results of the ray-tracing code).

The power reflection, transmission, and wave conversion coefficients through the ion-ion resonance layer are given in terms of η as follows:

a) wave coming from the low magnetic field side:

$$R_+ = (1 - e^{-2\eta})^2 \qquad T_+ = e^{-2\eta} \qquad A_+ = e^{-2\eta}(1 - e^{-2\eta}) \tag{12a}$$

b) wave coming from the high magnetic side:

$$R_- = 0 \qquad T_- = e^{-2\eta} \qquad A_- = 1 - e^{-2\eta} \tag{12b}$$

Here $A_\pm$ is the fraction of power which is mode converted; it is assumed that this power is totally absorbed by the particles. If Bernstein waves are excited which propagate *away* from the resonance, it is attributed entirely to the electrons. If on the contrary the cold shear wave is excited, it is attributed to the minority ions and to the electrons in proportion to their respective contribution γ_α to the antihermitean part of the dielectric tensor at the mode conversion point:

$$\begin{aligned} \gamma_e &= Cte \cdot n_F^2 \frac{\omega_{pe}^2}{\omega^2} \frac{v_{th,e}^2}{c^2} x_{oe} e^{-x_{oe}^2} \\ \gamma_i &= Cte \cdot \frac{1}{2} \cdot \left(\frac{(n_\parallel^2 - \mathcal{R}_o)}{(n_\parallel^2 - S_o)} \right)^2 \cdot \frac{\omega_{pm}^2}{\omega^2} x_{om} e^{-x_{1m}^2} \end{aligned} \tag{13}$$

where $x_{n,\alpha} = (\omega - n\Omega_\alpha)/k_z v_{th\alpha}$. The first factor in γ_i takes into account that only the E_+ component of the electric field is absorbed by the ions.

Direct ion cyclotron damping of the fast wave by the minority ions can be estimated by taking the spatial variation of the electric field from the solution of the Budden equation, and integrating the power transport equation through the Doppler broadened cyclotron layer. The parameter

$$\epsilon = 2n_\parallel^2 \frac{v_{th,m}^2}{c^2} \left[(n_\parallel^2 - S_o) \frac{\Omega_{cm}^2}{\omega_{pm}^2} \right]^2 \tag{14}$$

determines wether the wave is in the minority ($\epsilon >> 1$) or in the wave conversion ($\epsilon << 1$) regime. Both regimes are covered by writing the fractional absorption of the fast wave by the minority ions as

$$\alpha_m = \pi \frac{\epsilon}{1+\epsilon} n_F (k_o R_o) \cdot \left| \frac{(n_\parallel^2 - \mathcal{R}_o)}{(n_\parallel^2 - \mathcal{L}_o)(n_\parallel^2 - S_o)} \right| \cdot \frac{\omega_{pm}^2}{\Omega_{cm}^2} \tag{15}$$

Similarly, first harmonic damping by the majority species is given by:

$$\alpha_M = \frac{\pi}{2} \frac{\epsilon}{1+\epsilon} n_F^3 (k_o R_o) \cdot \left| \frac{(n_\parallel^2 - \mathcal{R}_o)}{(n_\parallel^2 - \mathcal{L}_o)(n_\parallel^2 - S_o)} \right| \cdot \frac{\omega_{pM}^2}{\Omega_{cM}^2} \frac{v_{th,M}^2}{c^2} \tag{16}$$

Near an ion-ion resonance α_M is of course only present when the first harmonic resonance of the majority species coincides with the fundamental of the minority. If on the other hand the minority species is absent (pure first harmonic heating), this same expression can be used with $\epsilon/(1+\epsilon) = 1$. (Eqs. (15) and (16) describe absorption of

the fast wave, while Eqs. (13) refer to the slow, mode converted wave; the two processes are assumed to be additive in this simple model, which might lead to a slight overestimation of absorption in the minority regime).

Finally, one has to account for Transit time damping by the electrons. This damping is not localised near resonances; rather, it is locally proportional to β:

$$\frac{d\log(P)}{dx} = \frac{\sqrt{\pi}}{2} k_o \cdot n_F \cdot \frac{\omega_{pe}^2}{\Omega_{ce}^2} \frac{v_{th,e}^2}{c^2} \cdot x_{o,e} e^{-x_{o,e}^2} \tag{17}$$

It is therefore rather strongly peaked towards the plasma center. This allows a rough estimate of the fractionas absorption taking place between two resonances (or between wall and a resonance):

$$\alpha_e(X_o) = \gamma_t \cdot (k_o^3 \cdot haR) \left\{ n_F \cdot \frac{\omega_{pe}^2}{\Omega_{ce}^2} \frac{v_{th,e}^2}{c^2} \cdot x_{o,e} e^{-x_{o,e}^2} \right\}_{X_o} \tag{18}$$

the quantities in brackett being taken at the resonance X_o; γ_t is a numerical factor to take into account profile effects, which is expected to lie between 0.1 and 0.5, and can be adjusted by comparison with Ray Tracing. These approximations should be good for resonances close to the plasma center, and bad for those at the periphery; near the latter however electron transit time damping is anyhow negligible.

2.4 - Evaluation of the single transit damping efficiency. Eqs. (12) to (16) allow a complete power balance of a single transit through the resonance layer. Depending on the relative position of cyclotron and wave resonances, and on the side of incidence of the wave, the fraction of incident power which flows into the different channels will be:

1a) Wave incident from the low magnetic field side, minority cyclotron resonance to the outside of the ion-ion resonance:

- to te electrons	$\alpha_e + \tau_e\tau_i\{(R_+\tau_i + T_+)\alpha_e + A_+\gamma_e\}$
- to minority ions	$\tau_e\{\alpha_m + \tau_i(R_+\alpha_m + A_+\gamma_i)\}$
- to majority ions	$\tau_e(\alpha_m + \tau_i R_+ \alpha_m)$
- reflected	$\tau_e\tau_i R_+ \tau_i\tau_e$
- transmitted	$\tau_e\tau_i T_+ \tau_e$

1b) Wave incident from the low magnetic field side, minority cyclotron resonance to the inside of the ion-ion resonance:

- to electrons	$\alpha_e + \tau_e\{A_+\gamma_e + (T_+\tau_i + R_+)\alpha_e\}$
- to minority ions	$\tau_e(A_+\gamma_i + T_+\alpha_m)$
- to majority ions	$\tau_e T_+\alpha_m$
- reflected	$\tau_e R_+\tau_e$
- transmitted	$\tau_e T_+\tau_i\tau_e$

2a) Wave incident from the high magnetic field side, minority cyclotron resonance to the outside of the ion-ion resonance:

- to the electrons	$\alpha_e + \tau_e\{A_-\gamma_e + (T_- + R_-\tau_i)\alpha_e\}$
- to minority ions	$\tau_e(A_-\gamma_i + T_-\alpha_m)$
- to majority ions	$\tau_e T_-\alpha_m$
- reflected	$\tau_e R_-\tau_e \qquad (= 0)$
- transmitted	$\tau_e T_-\tau_i\tau_e$

2b) Wave incident from the high magnetic field side, minority cyclotron resonance to the inside of the ion-ion resonance:

- to the electrons	$\alpha_e + \tau_e\tau_i\{A_-\gamma_e + (T_- + R_-\tau_i)\alpha_e\}$
- to minority ions	$\tau_e\{\alpha_m + \tau_i(A_-\gamma_i + T_-\alpha_m)\}$
- to majority ions	$\tau_e(\alpha_m + \tau_i T_-\alpha_m)$
- reflected	$\tau_e R_-\tau_i\tau_e \qquad (= 0)$
- transmitted	$\tau_e T_-\tau_e$

where

$$\tau_i = 1 - \alpha_m - \alpha_M \qquad \tau_e = 1 - \alpha_e$$

In each case the contributions sum to unity.

2.5 - Evaluation of the total power deposition. A simple algorithm also allows to estimate the power deposited into the electrons and the various ions species after a number of transits sufficient for complete absorption. The plasma diameter is divided into $N + 1$ regions by the N resonances to be crossed, and two arrays, $PTOLFT(j)$ and $PTORGT(j)$, are foreseen to contain, for each interval, the power *which has not yet been accounted for*, flowing to the left and to the right respectively. If for example the antenna is on the outer side, $PTOLFT(1)$ is initialised to $P(n_\phi)$, and all other elements to zero. The scattering scenario relevant to the first resonance is then applied: the absorbed power is attributed to the various species, the transmitted power is added to $PTOLFT(2)$, the reflected power to $PTORGT(1)$, and finally $PTOLFT(1)$ is reset

to zero. The same procedure can now be applied to the second region, $PTOLFT(2)$ now playing the role of incident flux, and so on, until the inner wall is reached. Upon reflection from the wall, a fraction α_w of $PTOLFT(N+1)$ can be assumed to be absorbed there (this might include losses in the scrape-off plasma, resistive losses in the vessel, radiation from the vessel apertures, etc.; moreover, α_w can be different for the inner and outer wall). Now $PTORGT(N+1)$ is initialised to $(1-\alpha_w)\cdot PTOLFT(N+1)$, and $PTOLFT(N+1)$ reset to zero, and the procedure is repeated towards the right, picking up the fluxes $PTORGT(j)$ from the previous transit, and so on, until absorption is complete.

It will be noted that this procedure is not strictly rigorous, since it assumes that the power fluxes of successive transits are additive, thereby excluding constructive or destructive interference effects occurring just near a resonance plane. This is at least partly justified by the fact that such effects, if present at all, must vary with vertical position, since the real geometry is far from being really plane-layered. Thus even if locally wrong, the estimate obtained in this way should be correct in an averaged sense.

2.6 - Power deposition profiles. The evaluation of the power deposition profiles is optional and very crude. With reference to Fig. 2, the inner and outer magnetic surfaces cut by the illuminated region of a resonance layer are approximately labeled

$$\psi_1 = \frac{X_o - R_a}{a} \qquad \psi_2 = \left(\frac{(X_o - R_a)^2}{a^2} + \frac{h^2}{b^2}\right)^{1/2} \tag{17}$$

($\psi = 0$ on the magnetic axis, $\psi = 1$ on the plasma edge). $X_o - R_a$ is the distance of the resonance from the magnetic axis, h the half-height of the waves beam, a and b the horizontal and vertical radii of the plasma. For each resonance layer, the absorbed power is distributed according to a cosinus squared law, with maximum in ψ_1 and zero in ψ_2. To obtain the power density, the volume of the plasma layer between ψ and $\psi + \Delta\psi$ is taken to be

$$\Delta V = (2\pi R_a) \cdot (\pi ab) \cdot \psi \Delta\psi \tag{18}$$

These very rough estimates could be improved both by taking into account Doppler broadening, and by describing better the plasma geometry. It is however doubtful wether the results would thereby be made more accurate, since the largest uncertainty comes from the assumed spatial distribution of the power flux incident upon the resonance layer, about which a better guess is hardly available.

3. - Comparison with Ray tracing.

In this section we present some results obtained with ICEVAL, and we compare them with the predictions of a Ray Tracing code for the same situations. The Ray Tracing results are taken from [6], where a more detailed discussion of the physics can also be found. Here we concentrate on the comparison, in order to reach a better understanding of the possibilities and limitations of the simple model developed in the previous Section. For convenience, the relevant figures from [6] are reported whenever useful (a few cases have been re-run to take advantage of improvements made to the the Ray Tracing code after the publication of [6]). The parameters for the plasma and the antenna are summarised in Table 1; in the following, we will mention only those parameters which are varied with respect to the standard ones listed there.

3.1 - The antenna spectrum. Fig. 3 shows the comparison of the n_ϕ spectrum radiated by the antenna according to ICEVAL with the antenna model built in the Ray Tracing code [6] at $f = 35$ Mhz. To obtain a good simulation, we had to take $\eta_o = 0.2$ in Eq. (4), about a factor 1.5 smaller than the direct estimate. This means that the model spectrum of section 2.2 is not very accurate, a fact which is not be very astonishing, as no allowance was made for the variation of the plasma surface admittance with n_z. On the other hand the same value for η_o gives a good simulation of both the dipole and quadrupole antenna, and at different frequencies (the spectrum predicted at $f =$ 50 Mhz is shown in Fig. 13).

3.2 - He_3^{++} minority in an Hydrogen plasma. As a first example, we have applied ICEVAL to the case of an isolated ion-ion resonance. In the case of He_3^{++} in Hydrogen, the cyclotron resonance of the minority ions lies between the antenna and the mode conversion layer, a situation which favors minority heating at low concentrations; due to the large dimensions of the JET plasma, however, the optical thickness of the evanescence layer between cut-off and resonance layer becomes large as soon as the mode conversion regime is reached, so that above a few percent concentration absorption becomes relatively weak.

The single transit absorption by He_3^{++} and electrons as a function of the minority concentration are compared in figs. 4a (Ray Tracing) and 4b (ICEVAL) for a dipole antenna, and by figs. 5a and 5b for a quadrupole antenna. The behaviour as function of temperature for a fixed He_3^{++} concentration are compared in Figs. 6a and 6b. In all these runs of ICEVAL the constant γ_o of Eq. (9) was taken equal to 1.333; variations with γ_o are however not large in the range $1 \lesssim \gamma_o \lesssim 2$.

Although agreement between ICEVAL and Ray Tracing is generally quite good, there are considerable differences in details. On the whole, the simple model tends to predict an excessively sharp transition between minority and mode conversion regimes, and therefore a reduced electron heating in transition situations compared to the Ray Tracing results. The most likely explanation for this behaviour is that the simple model ignores the considerable broadening and mixing of the $k_{||}$ spectrum occurring in the real configuration due to refraction and to the vertical variation of the poloidal component of the static magnetic field. Spectral broadening makes the distinction between the two regimes in the real configuration much less clear-cut than assumed in the slab model, and favours electron heating. In addition, the sensitivity of minority cyclotron damping on temperature seems to be somewhat underestimated by ICEVAL, possibly because the simplified model for the screening of the E_+ component of the h.f. field is not very accurate; it is however difficult to separate this effect from the previous one.

In Fig. 7 the repartition of the power between the various channels after total absorption is shown as function of the He_3^{++} concentrations, for the same parameters as in Figs. 4. A fraction equal to 5% and 1% of the power incident on the outer and inner wall respectively was assumed to be lost at each reflection. As expected, most of the power goes to the channel for which the first transit absorption is already the largest; the sharpness of the transition between minority and mode conversion regimes is further enhanced by this effect. Perhaps the most interesting feature of these results is the fact that above a minority concentration of a few percent a very large fraction of the power can be expected to be deposited directly into the electrons. Since the single transit damping is relatively weak in this regime, a correspondingly larger h. f. reactive energy will be present in the plasma.

A total power absorption balance of this kind is beyond the possibility of Ray Tracing: a check of these results would require extensive runs of a Full Wave code, with the inclusion of wall losses. In practice, a rough estimate as done in ICEVAL, gauging the wall losses from the measured heating efficiency, is probably as much as can be done at present.

3.3 - Harmonic Heating of Deuterium. The density and temperature dependence of the first transit absorption are compared in Figs. 8a, 9a (Ray Tracing) and 8b, 9b (ICEVAL), respectively. Deuterium harmonic damping is expected to be roughly proportional to the value of β, hence approximatively linear with both n_e and T: this is well reproduced by the simple model. The optical thickness of the evanescence layer which screens the mode conversion layer from the cyclotron harmonic resonance of Deuterium increases with β, so that electron heating by Bernstein Waves saturates

and even decreases at large density and temperature. The further increase of electron heating found by Ray tracing is not localised near resonance; rather, it is due to the onset of electron transit time damping. To achieve a good simulation of this effect in the simplified model, we had to put $\gamma_{tte} = 0.1$ in Eq. (18), close to the lower limit of the theoretical estimate.

3.4 - Hydrogen minority in Deuterium. In this important heating scenario, the variation of the first transit absorption on the H^+ concentration and on temperature predicted by Ray Tracing (Figs. 10a and 11a, respectively) are remarkably well reproduced by ICEVAL (Figs. 10b and 11b). The same value of γ_{tte} as in the previous case was used to simulate electron transit time damping. Above about 4 keV, this effect is found to deplete significantly the power flux reaching resonance, so that H^+ heating saturates. We note that the inclusion of electron transit time damping in the simple model is essential, for without it electron heating as predicted by ICEVAL would have the wrong dependence upon temperature. However, the rough way in which it is simulated will lead to some distortion of the electron power deposition profile at high temperature.

A closer comparison also shows that ICEVAL predicts a considerably larger damping by minority ions at very low concentrations (below about 1%), compared with the Ray Tracing code. In the minority regime ICEVAL is likely to overestimate somewhat cyclotron damping, as already stated; moreover, the first transit results of ICEVAL include also cyclotron damping of the wave *reflected* from the mode conversion layer, in contrast to those of the Ray Tracing code. These are however small effects, particularly when the minority concentration is very low. Once more, the approximation for the field polarisation seems to be the main source of disagreement. It must however be stated that for very low values of the minority concentration, the step used in the Ray Tracing code to integrate the ray equations (which is automatically determined by a predictor-corrector subroutine on the sole criterion of accuracy), might be so large that for small values of $n_{||}$ the cyclotron resonance layer might just not be seen. Thus minority heating could be somewhat underestimated under these circumstances by Ray Tracing in [6], and the ICEVAL results could be closer to reality. Fortunately, this problem with the Ray Tracing code is restricted to a range of insignificantly low H^+ concentrations.

It is also interesting to compare the first transit absorption with the total absorption, the latter being shown in Fig. 12 as a function of the central electron temperature at a fixed H^+ concentration. Electron heating is considerably enhanced with respect to the first transit results: this is due to the fact that the wave reflected from the inner wall

and incident upon the resonance from the high magnetic field side has a much higher mode conversion efficiency than the wave coming directly from the antenna.

Fig. 13 shows the power spectra radiated and absorbed in the first transit (13a) and after complete absorption (13b) (5% H^+, T = 1.7 keV). A characteristics of these results is the large amount of power going into the wall for low values of $n_{||}$: it can be recognised from the difference between the radiated and the sum of absorbed power. Although spectral broadening should somewhat improve the situation in the experimental situation, this is likely to be a real effect. The important question wether this result could be related to impurity production, and in the affirmative wether shaping of the $n_{||}$ spectrum could be beneficial [8], would requires closer investigation.

Fig. 14 finally displays an example of radial power deposition profiles, as obtained by ICEVAL, for one of the cases of Fig. 10a (H^+ concentration of 5%). The large values near the plasma center are a well known geometric effect. In spite of the rough approximations made, these profiles ressemble those obtained by Ray Tracing (fig. 14b), and would be quite adequate for example as input in a transport simulation code.

Acknowledgments.

We whish to thank Dr. P. Lallia for suggesting the present work. To him and to Dr. Noterdaeme we are also indebted for several useful suggestions about its realisation.

Appendix: The Subroutine ICEVAL.

The subroutine ICEVAL is about 500 FORTRAN lines long, and takes a small (< 0.1) fraction of a second on a CRAY 1 computer to run a single case. It makes no call to other subroutines, and has no internal STOP point. If the case cannot be evaluated, for example because of inconsistencies of the input data, a diagnostic is printed, followed by a RETURN to the calling program.

We now describe briefly the input and output of the subroutine ICEVAL, to facilitate its use. All input and output quantities have been grouped into the following three labelled commons (plus a few parameters), which of course must appear also in the user program (ICEVAL itself has no arguments):

```
PARAMETER (NSP=2), (NSP2=2*(NSP+1)), (NZDIM=25), (NPSI=50)
COMMON /INPICV/ RTORUS, RPLASM, DMAXIS, ELLIPT, BZERO,
                DENC,   TEMPEC, FREQCY, POWER,  EPHASE,
                DISTAP, DISTAW, WIDTH,  HEIGHT, WGAP,
                AWALLE, AWALLI,
                TEMPIC(NSP),    ATM(NSP),       AZI(NSP),
                ACONC(NSP),     NSPEC,  ISIDE,  JPOLE
COMMON /CTRICV/ EVANT,  ANGLCO,
                NPHMAX, JUMPHI, IANT,   JOUTA,  IPWRAD
COMMON /OUTICV/ ANZ(NZDIM),     PWCPL(NZDIM),
                PWE1(NZDIM),    PWI1(NSP2,NZDIM),
                PWE(NZDIM),     PWI(NSP2,NZDIM),
                PSI(NPSI),      PSPWE(NPSI),
                PSPWI(NSP,NPSI),
                PFRST,  PFRSTE, PTOTE,  PWALLE, PWALLI,
                PFRSTI(NSP),    PTOTI(NSP),     NUMPHI
```

The variables in the INPICV and CTRICV are input data to ICEVAL, and must therefore be defined by the user program *before* calling ICEVAL itself. The variables in OUTICV are the quantities evaluated by ICEVAL, which are thereby made available to the user code upon return from this subroutine. We now list these quantities with a few words of explanations for each.

a) Parameters. The following parameters are used so that array dimensions can be easily modified according to needs.

NSP: dimension of the arrays whose index runs over the ion species (the actual number of ion species is NSPEC, cfr. below).

NSP2: dimension of the arrays whose index runs over the possible resonance layers. NSP2 must be *not smaller* than $2 \cdot NSP + 2$.

NZDIM: dimension of the arrays whose index runs over toroidal modes (the actual number of modes is NUMPHI, cfr. below).

NPSI: dimension of the arrays whose index runs over the points of the radial mesh (NPSI is also the actual number of points used).

b) Common INPICV. The labeled common INPICV contains the quantities characterising the plasma equilibrium and the h.f. parameters for the case which must be run:

RTORUS: toroidal radius (to the geometrical center of the plasma) in cm.

RPLASM: horizontal plasma radius (half-diameter) in cm.

DMAXIS: displacement of the magnetic axis (positive to the outside) in cm.

ELLIPT: ellipticity (b/a), dimensionless.

BZERO: magnetic field in the center of the plasma, in Tesla.

DENC: electron density in the center of the plasma, in cm^{-3} (all profiles are assumed parabolic).

TEMPEC: electron temperature in the center of the plasma, in keV.

FREQCY: applied frequency, in Hz.

POWER: launched power, in MW (if POWER = 1, all other powers in the output can be interpreted as efficiencies).

EPHASE: for a quadrupole antenna (cfr. JPOLE below) phase difference between the two conductors, in degs.

DISTAP: distance between the antenna and the plasma edge (i.e the separatrix or limiter radius), in cm.

DISTAW: distance between the antenna and the wall or the return conductor, in cm.

WIDTH: width of each antenna conductor, in cm.

HEIGHT: half length of the antenna conductors in the poloidal direction, in cm.

WGAP: in the case of the quadrupole antenna, separation between the two conductors, in cm.

AWALLE: fraction of power lost on the outer wall on each reflection (dimensionless; must be less than unity).

AWALLI: fraction of power lost on the inner wall on each reflection (dimensionless; must be less than unity).

TEMPIC: array of dimension NSP for the ion temperatures in the center of the plasma, in keV.

ATM: array of dimension NSP for the atomic masses of the ions (atomic units).

AZI: array of dimension NSP for the charges of the ions (atomic units).

ACONC: array of dimension NSP for the concentrations of the ion species: ACONC(j) $= n_j/n_e$. Note that ACONC(1) needs not to be specified: *the species with index 1 must be the majority species.* Its concentration is evaluated within ICEVAL to satisfy charge neutrality.

NSPEC: number of ion species present. Should not exceed NSP.

ISIDE: specifies wether the antenna is on the outside (ISIDE $= 1$) or on the inside (ISIDE $= -1$) of the vesssel.

JPOLE: specifies wether the antenna is of the dipole (JPOLE $= 1$) or quadrupole (JPOLE $= 2$) type.

c) Common CTRICV. CTRICV contains control parameters:

EVANT: numerical factor in the estimate of evanescence below the R cut-off (cfr. Eq. (4) in the text). Suggested value $\simeq 0.25$.

ANGLCO: numerical factor taking into account the average inclination of wavefronts in the estimate of the optical thickness of ion-ion resonance layers (cfr. Eq. (10) in the text). Suggested value $\simeq 1.33$.

NPHMAX: largest toroidal wavenumber to be considered (typically between 40 and 60).

JUMPHI: step in the loops over the toroidal wavenumber. Suggested value 4. Note that 2·NPHMAX/JUMPHI + 1 must not exceed NZDIM.

IANT: specifies when the antenna spectre has to be evaluated. For this purpose, it *must* be put to 1 before the first call of ICEVAL, which sets it to zero after evaluating the spectrum, so that several cases with the same antenna and different plasma parameters can be successively run. If the paramters of the antenna are also changed, it must be reset to 1 by the user program.

JOUTA: specifies the level of details in the printed output from ICEVAL, increasing from 0 to 2: JOUTA = 0: only the single pass and global absorptions; JOUTA = 1: also the spectral distributions and the radial power distribution profiles (if evaluated). JOUTA = 2 gives detailed information on each resonance layer.

IPWRAD: specifies wether the radial power deposition profiles have to be evaluated (IPWRAD = 1) or not. If evaluated, they are also printed only if JOUTA $\geq$ 1.

d) Common OUTICV. The labelled common OUTICV contains the output from ICEVAL:

ANZ: array of dimension NZDIM containing the values of the parallel index $n_{||}$ of partial waves.

PWCPL: array of dimension NZDIM containing the spectral repartition of the radiated power among partial waves.

PWE1: array of dimension NZDIM containing the power absorbed by the electron from each partial wave *upon the first transit.*

PWI1: double array of dimensions NSP2 and NZDIM containing the power absorbed by the ions from each partial wave *upon the first transit.*

PWE: array of dimension NZDIM containing the total power absorbed by the electron from each partial wave.

PWI: double array of dimensions NSP2 and NZDIM containing the total power absorbed by the ions from each partial wave.

PSI: array of dimension NPSI containing the values of ψ $(0 < \psi < 1)$ at which the power deposition profiles are evaluated.

PSPWE: array of dimension NPSI containing the power absorbed by the electrons in W/cm^3 versus PSI.

PSPWI: double array of dimensions NSP2 and NPSI containing the power absorbed by the ions in W/cm^3 versus PSI.

PFRST: power absorbed *in the first transit* (summed over n_ϕ and species, MW).

PFRSTE: total power absorbed by the electrons *in the first transit* (summed over n_ϕ, MW).

PFRSTI: array of dimension NSP containing the total power absorbed by the ions *in the first transit* (summed over n_ϕ, MW).

PWALLE: total power dissipated in the outer wall (MW).

PWALLI: total power dissipated in the inner wall (MW).

PTOTE: total power absorbed by the electrons (MW).

PTOTI: array of dimension NSP containing the total power absorbed by the ions (MW).

NUMPHI: number of toroidal partial waves effectively present in the arrays ANZ, PWCPL, PWE1, PWI1, PWE, PWI.

Finally we note that ICEVAL provides printed output only; plots are considered to be the charge of the user program, in order to increase portability. The MAIN program installed at IPP produces plots of most of the output quantities from ICEVAL.

References.

[1] - M. Brambilla, Ray Tracing of Lower Hybrid and Ion Cyclotron Waves, Comp. Physics Rep. **4**, 71, 1986 (Proc. 3d Europ. Workshop on Problems in the Numerical Modeling of Plasmas, Varenna 1985, K. Appert editor).

[2] - L. Villard, K. Appert, R. Gruber, J. Vaclavik, Global Waves in Cold Plasmas, ibid. p. 95.

[3] - A. Fukuyama, K. Itoh, S.-I. Itoh, Global waves in Hot Plasmas, ibid. p. 137.

[4] - K.G. Budden, Radio Waves in the Ionosphere, Cambridge Univ. Press 1955, Ch. 21.

[5] - M. Brambilla, M. Ottaviani, Plasma Physics and Contr. Fus. **27**, 1, 1985.

[6] - M. Brambilla, Ion Cyclotron Heating of the Jet Plasma, Report IPP 4/217, April 1984.

[7] - M. Brambilla, to be published.

[8] - K. Itoh, A. Fukuyama, S.-I. Itoh, Comments Plasma Phys. Contr. Fus. **10**, 1986, 91.

TABLE I

a) Plasma parameters for the standard run:

Toroidal radius	300 cm
Plasma radius	120 cm
Shift of the magnetic axis	18 cm
Ellipticity	1.4
Central electron density	$5\ 10^{13}\ cm^{-3}$
Central temperature	1.7 KeV

b) Antenna parameters for the standard run:

Frequency:	He_3^{++}	35 Mhz
	D^+	50 Mhz
	D^+ with H^+	50 Mhz
Antenna on the outer side:		
Distance antenna-plasma		5 cm
Width of the antenna (toroidally)		15 cm
Half-length of the antenna (poloidally)		80 cm
Gap between conductors *(quadrupole only)*		5 cm
Phase between conductors *(quadrupole only)*		180°

Figure captions.

Fig. 1 - Example of rays and wavefronts for a JET plasma (5% H^+ in Deuterium). The cyclotron resonance is situated 5 cm to the inside of the magnetic axis.

Fig. 2 - Geometrical approximations for the evaluation of the power deposition profiles.

Fig. 3 - Exact and approximated ($\eta_o = 0.25$) antenna spectra at 35 Mhz.

Fig. 4 - First transit damping versus He_3^{++} concentration in a hydrogen plasma, dipole antenna,$\gamma_o = 1.333$: a) from Ray Tracing; b) from ICEVAL.

Fig. 5 - First transit damping versus He_3^{++} concentration, quadrupole antenna: a) from Ray Tracing; b) from ICEVAL.

Fig. 6 - First transit damping versus temperature (2% He_3^{++}), dipole antenna: a) from Ray Tracing; b) from ICEVAL.

Fig. 7 - Repartition of the damping after total (multitransit) absorption, versus He_3^{++} concentration.

Fig. 8 - First transit damping versus density in Harmonic Cyclotron heating of a pure D^+ plasma, dipole antenna: a) from Ray Tracing; b) from ICEVAL.

Fig. 9 - First transit damping versus temperature in Harmonic Cyclotron heating of a pure D^+ plasma, dipole antenna: a) from Ray Tracing; b) from ICEVAL.

Fig. 10 - First transit damping versus H^+ concentration in a Deuterium plasma, dipole and quadrupole antennas: a) from Ray Tracing; b) from ICEVAL.

Fig. 11 - First transit damping versus temperature (5% H^+ in Deuterium), dipole antenna: a) from Ray Tracing; b) from ICEVAL.

Fig. 12 - Total damping versus temperature (5% H^+ in Deuterium), dipole antenna: a) from Ray Tracing; b) from ICEVAL.

Fig. 13 - Radiated and absorbed spectra (5 % H^+ in Deuterium), dipole antenna: a) first transit; b) total.

Fig. 14 - Radial power deposition profiles for 5% H^+ in Deuterium, other parameters as in Fig. 10a, dipole antenna. a) from ICEVAL; b) from Ray Tracing.

N_φ = 0.00

ΔS = 0.50

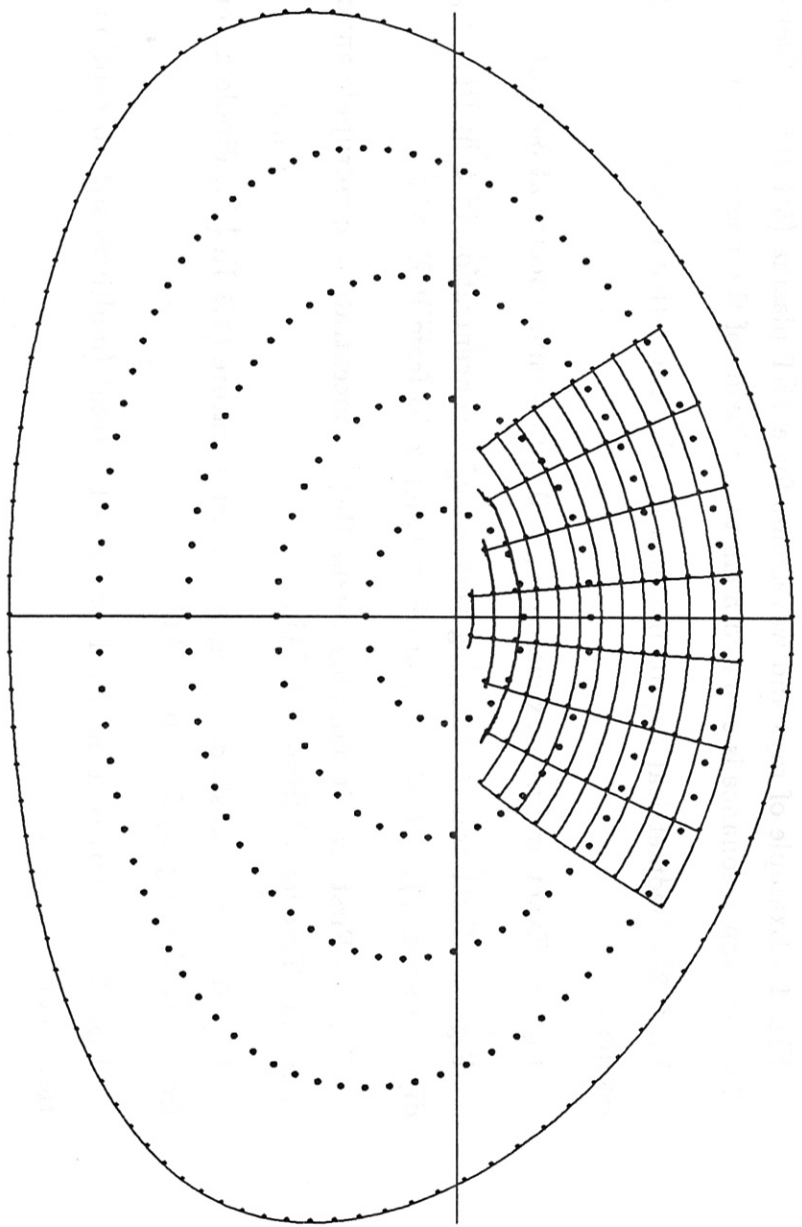

FIG. 1

FIG. 2

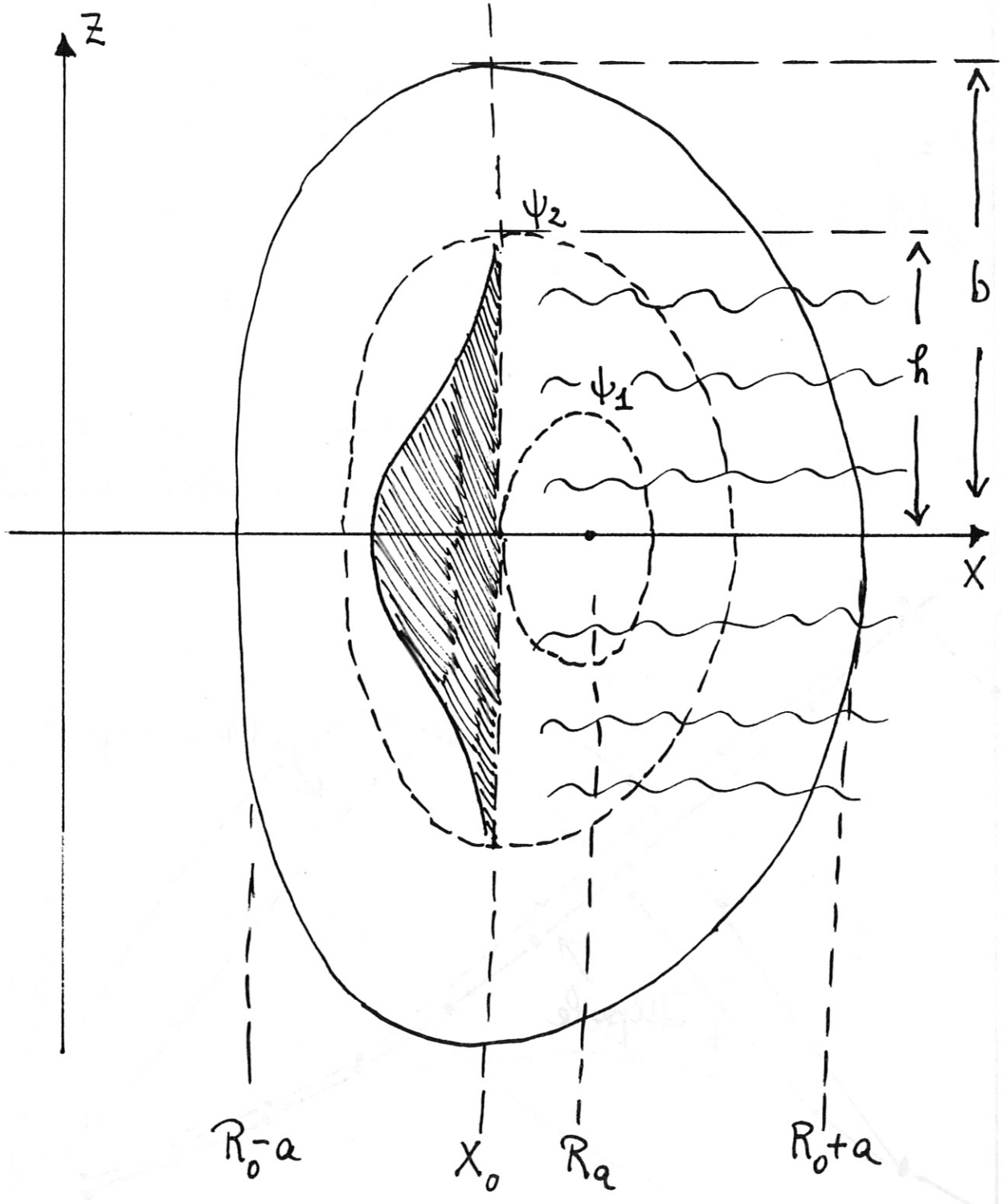

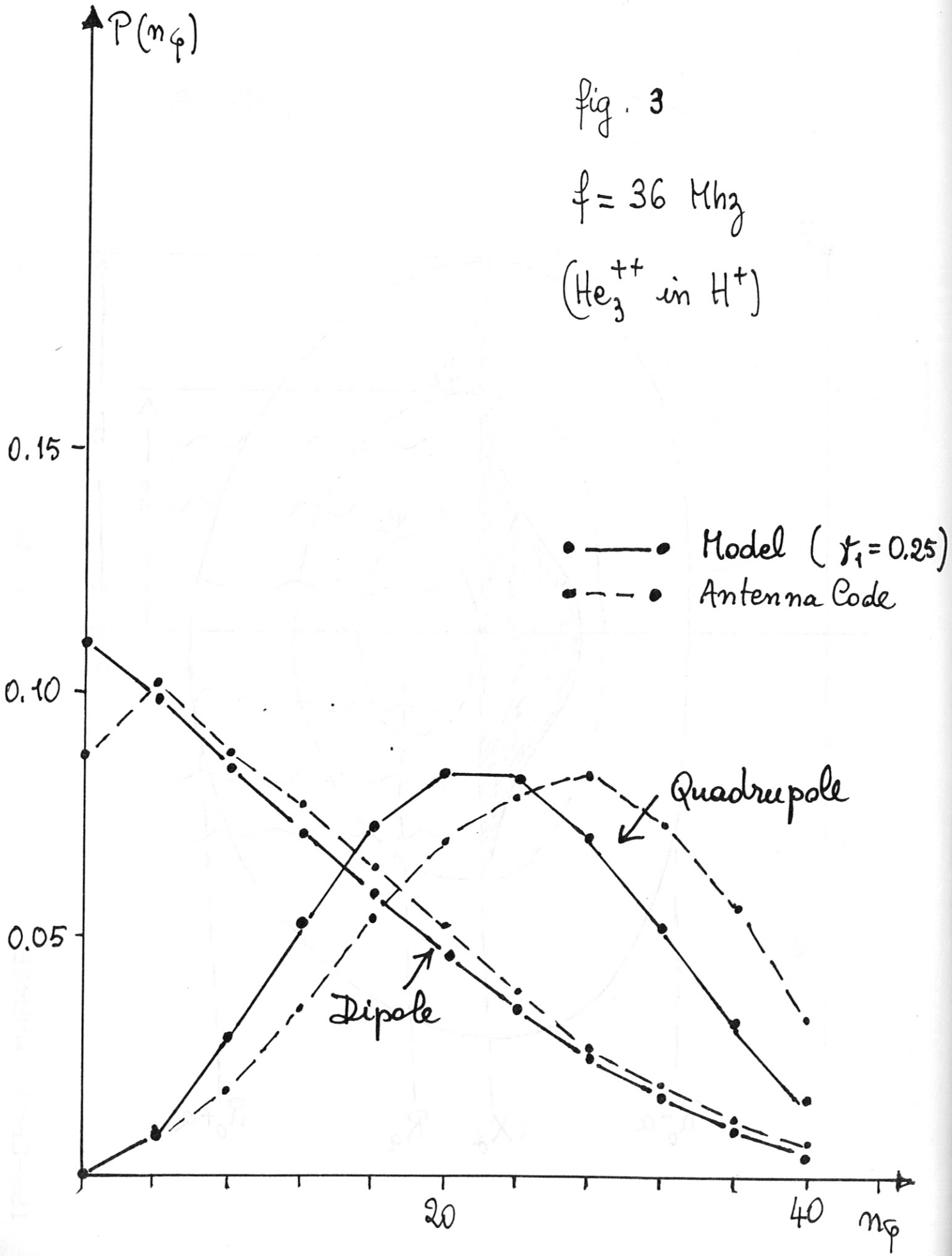

fig. 3

f = 36 Mhz

(He_3^{++} in H^+)

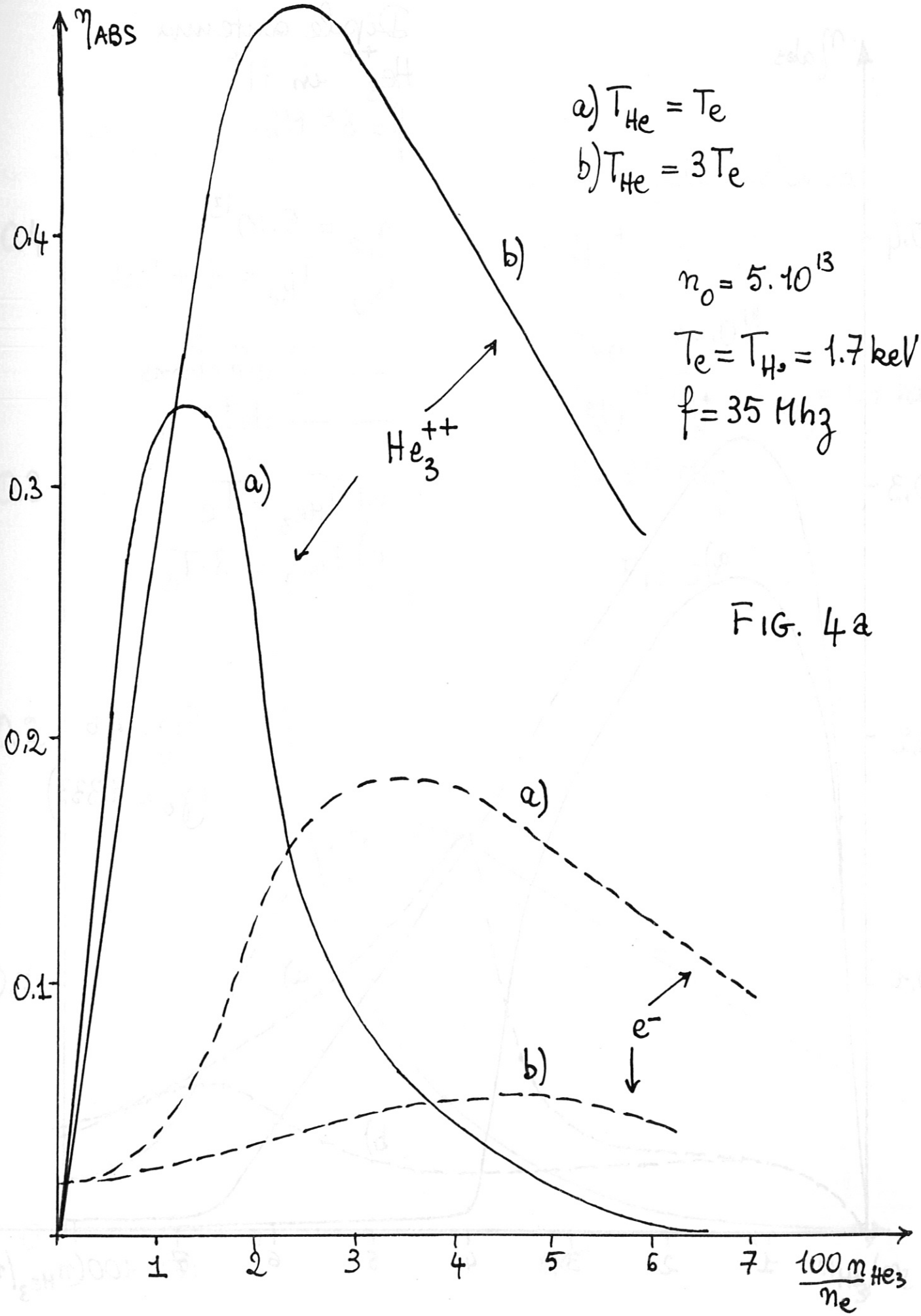
η_{ABS}
a) $T_{He} = T_e$
b) $T_{He} = 3T_e$
$n_0 = 5.10^{13}$
$T_e = T_{H_2} = 1.7$ keV
$f = 35$ Mhz
0.4
0.3
0.2
0.1
b)
a)
He_3^{++}
a)
e^-
b)
1
2
3
4
5
6
7
$\frac{100\, n_{He_3}}{n_e}$

FIG. 4a

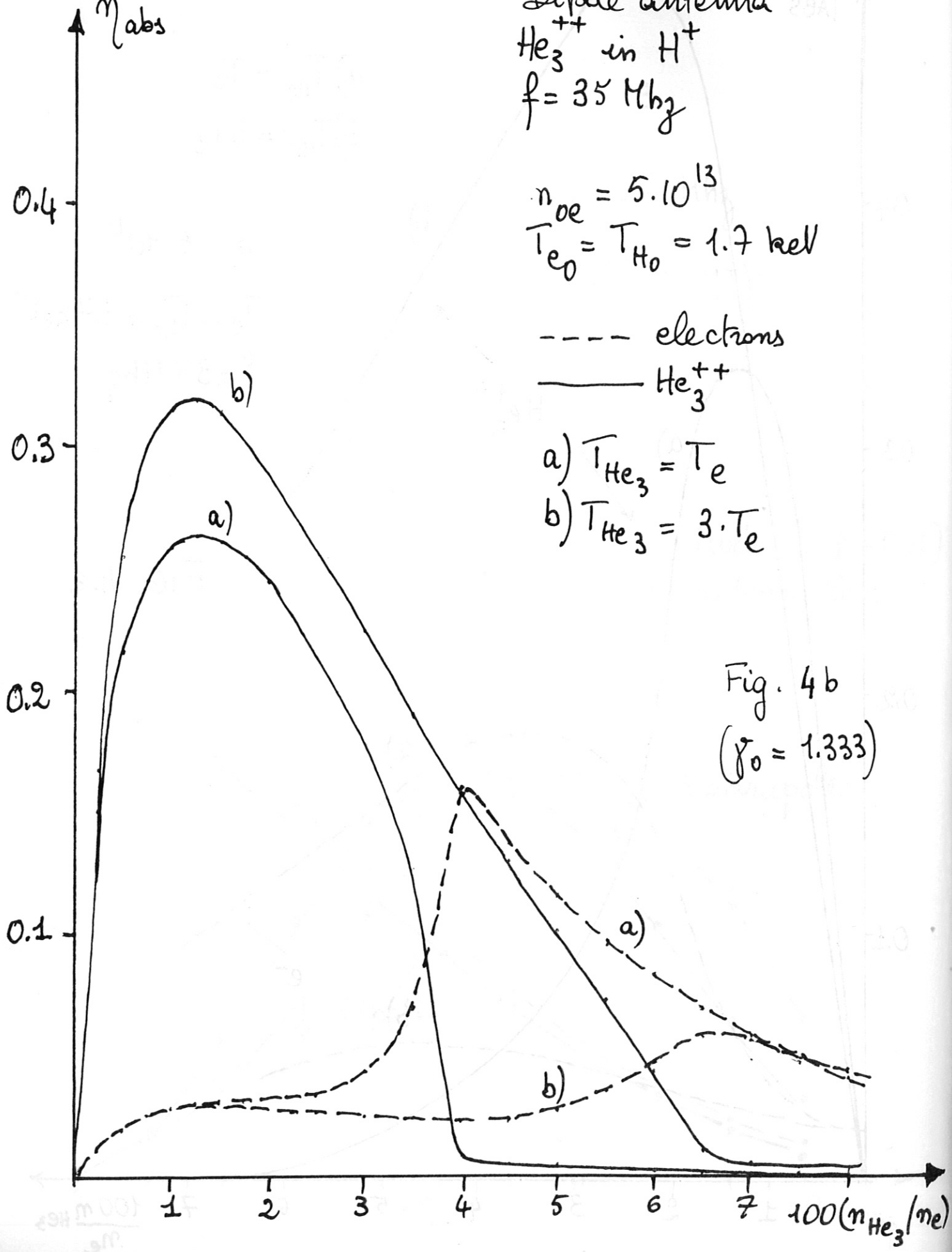

Fig. 4b
($\gamma_0 = 1.333$)

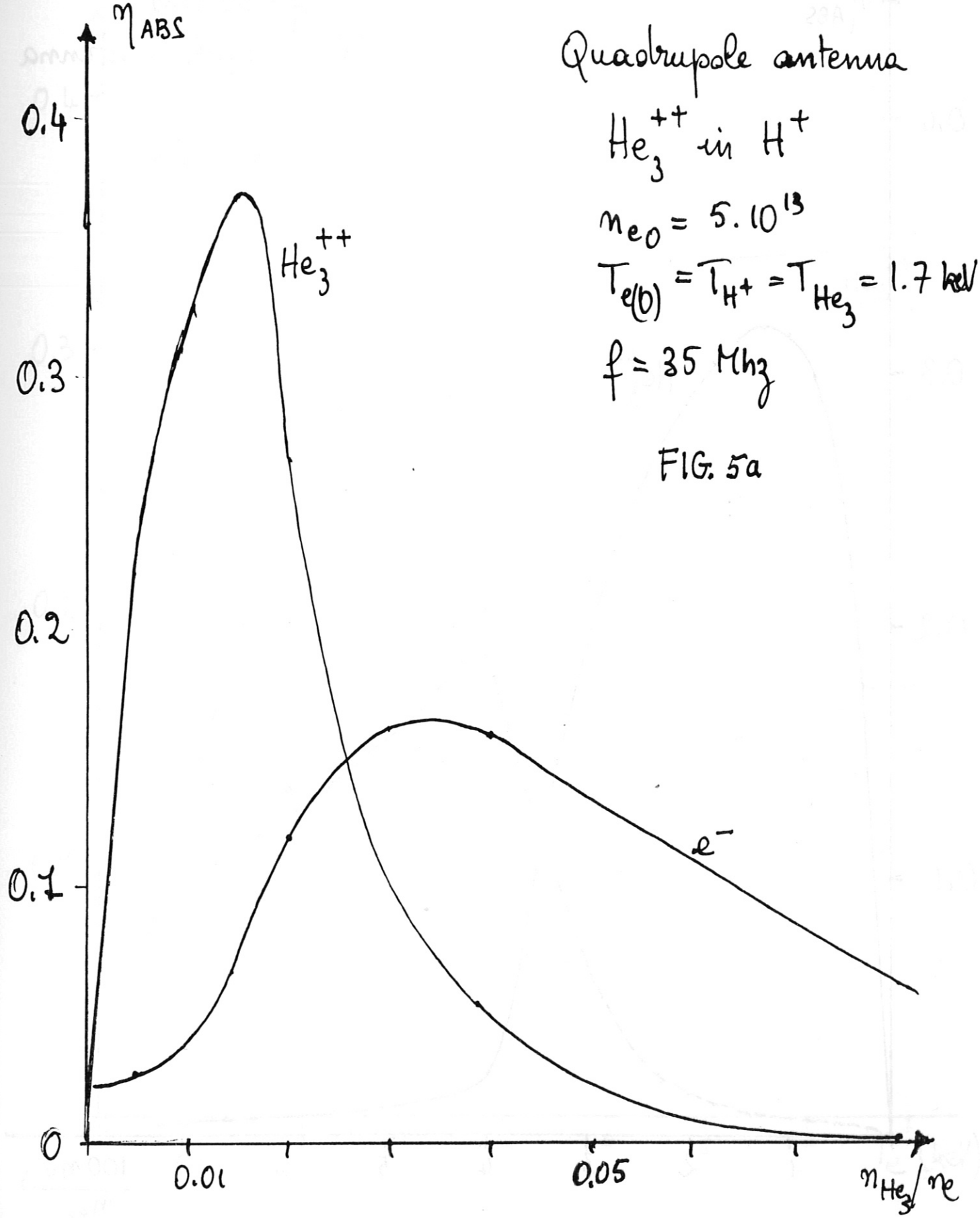

Quadrupole antenna

He_3^{++} in H^+

$n_{e0} = 5.10^{13}$

$T_{e(0)} = T_{H^+} = T_{He_3} = 1.7$ keV

$f = 35$ Mhz

FIG. 5a

He_3^{++} in H^+
$f = 35$ Mhz
Quadrupole antenna

FIG. 5b

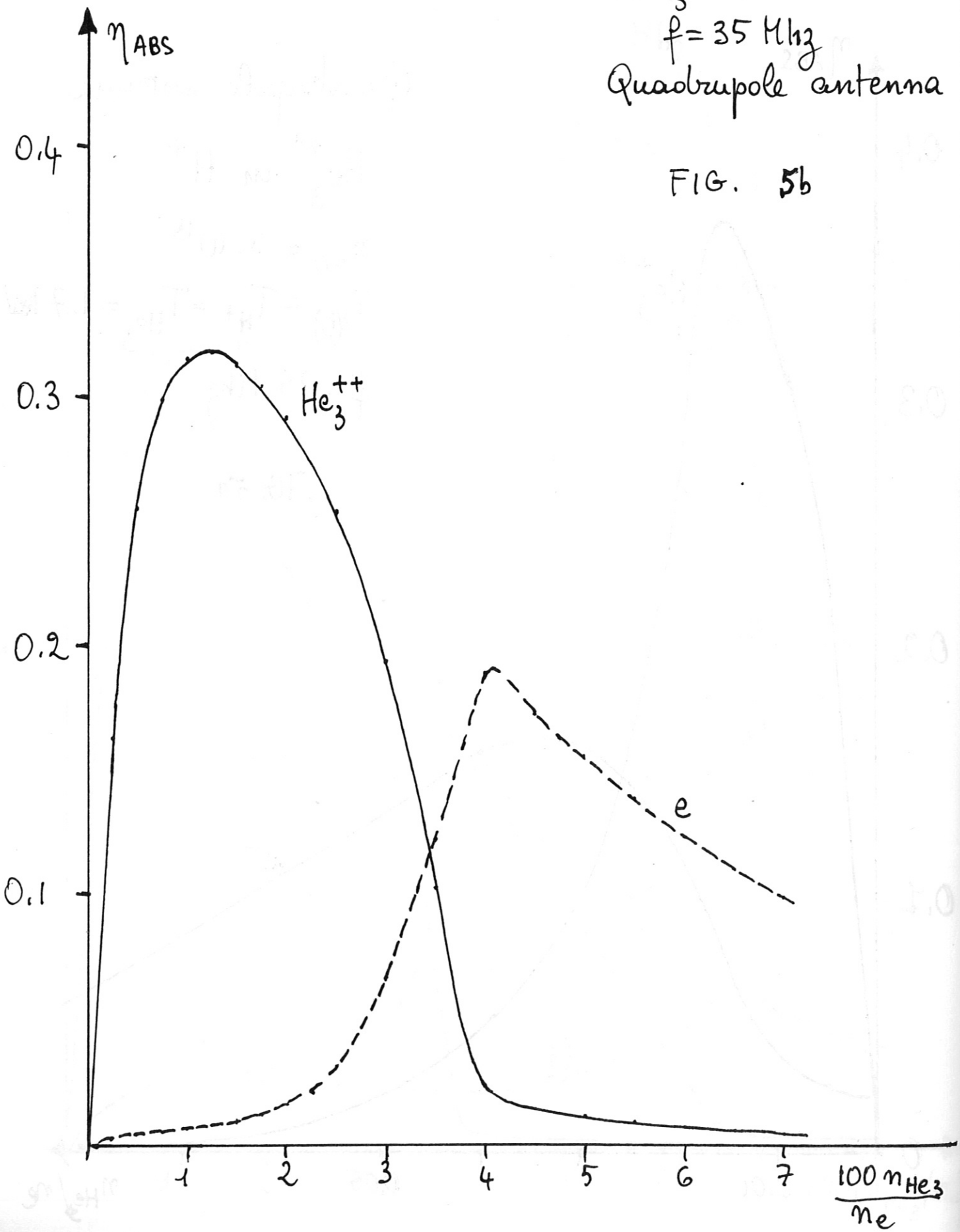

$n_e = 5 \cdot 10^{-3}$

$n_{He_3} / n_e = 0.02$

FIG. 6a

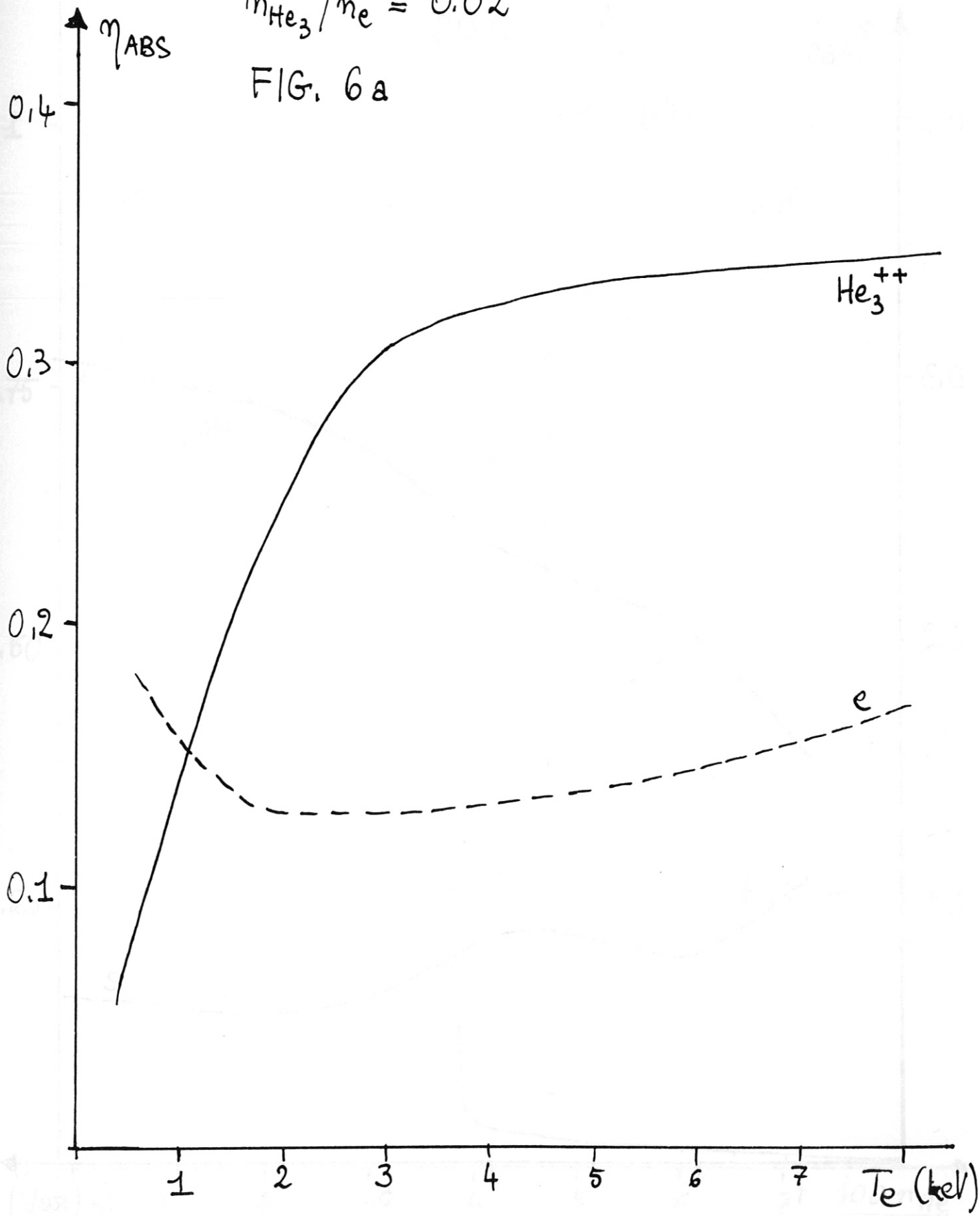

$n_e = 5 \cdot 10^{-3}$

$n_{He_3}/n_e = 0.02$

Fig. 6b

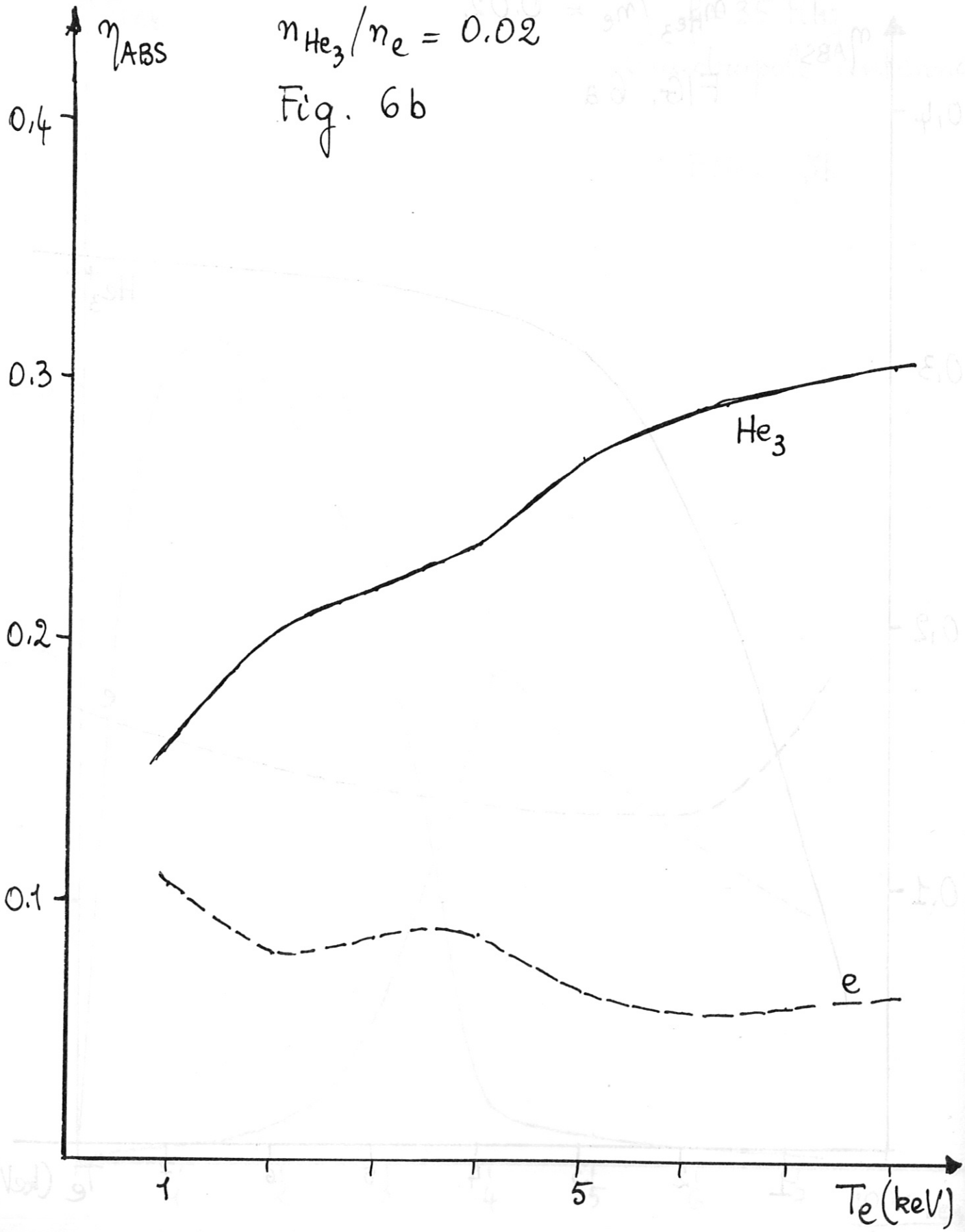

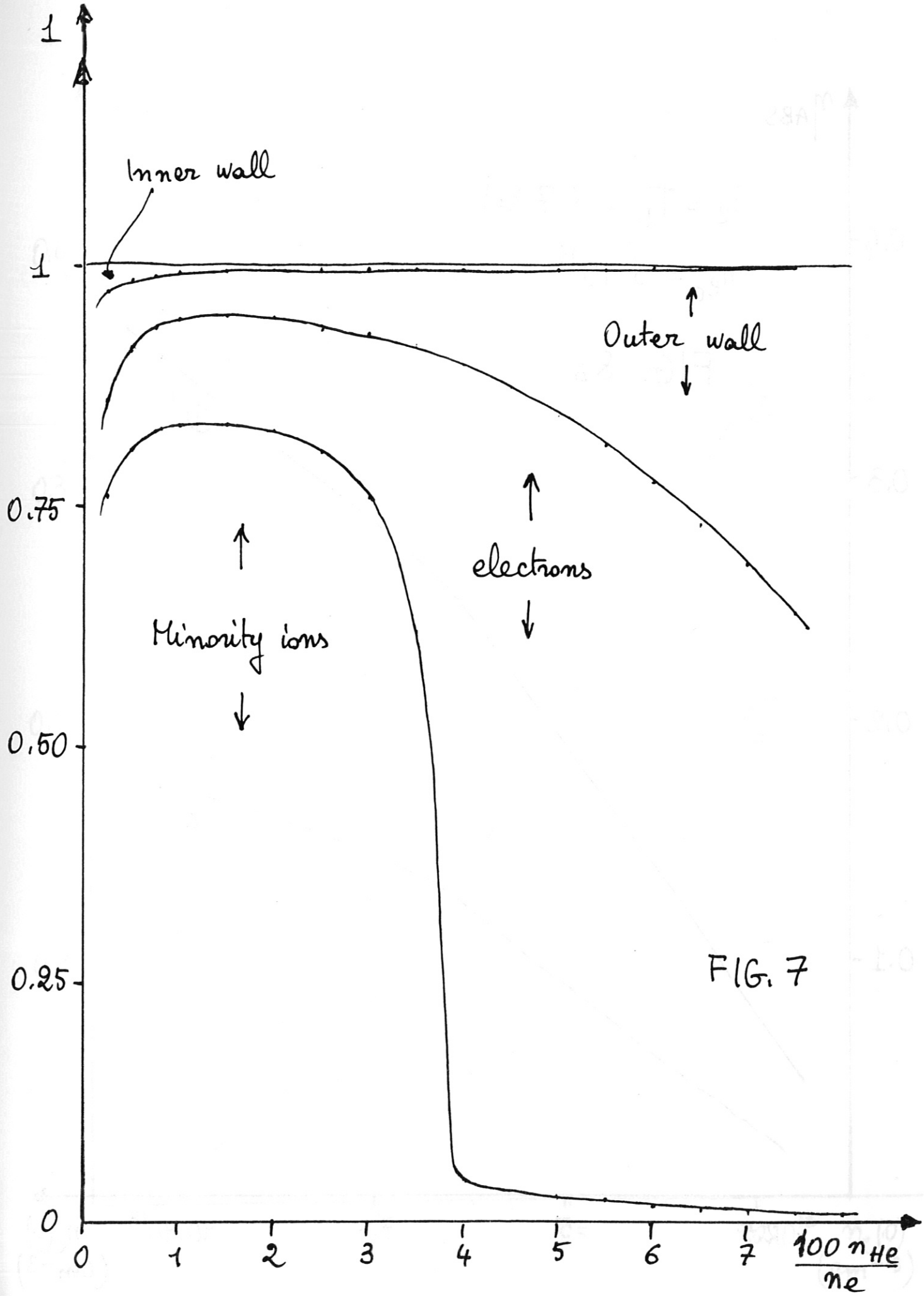
1
Inner wall
1
Outer wall
0.75
electrons
Minority ions
0.50
0.25
0
0
1
2
3
4
5
6
7
100 n He / ne

FIG. 7

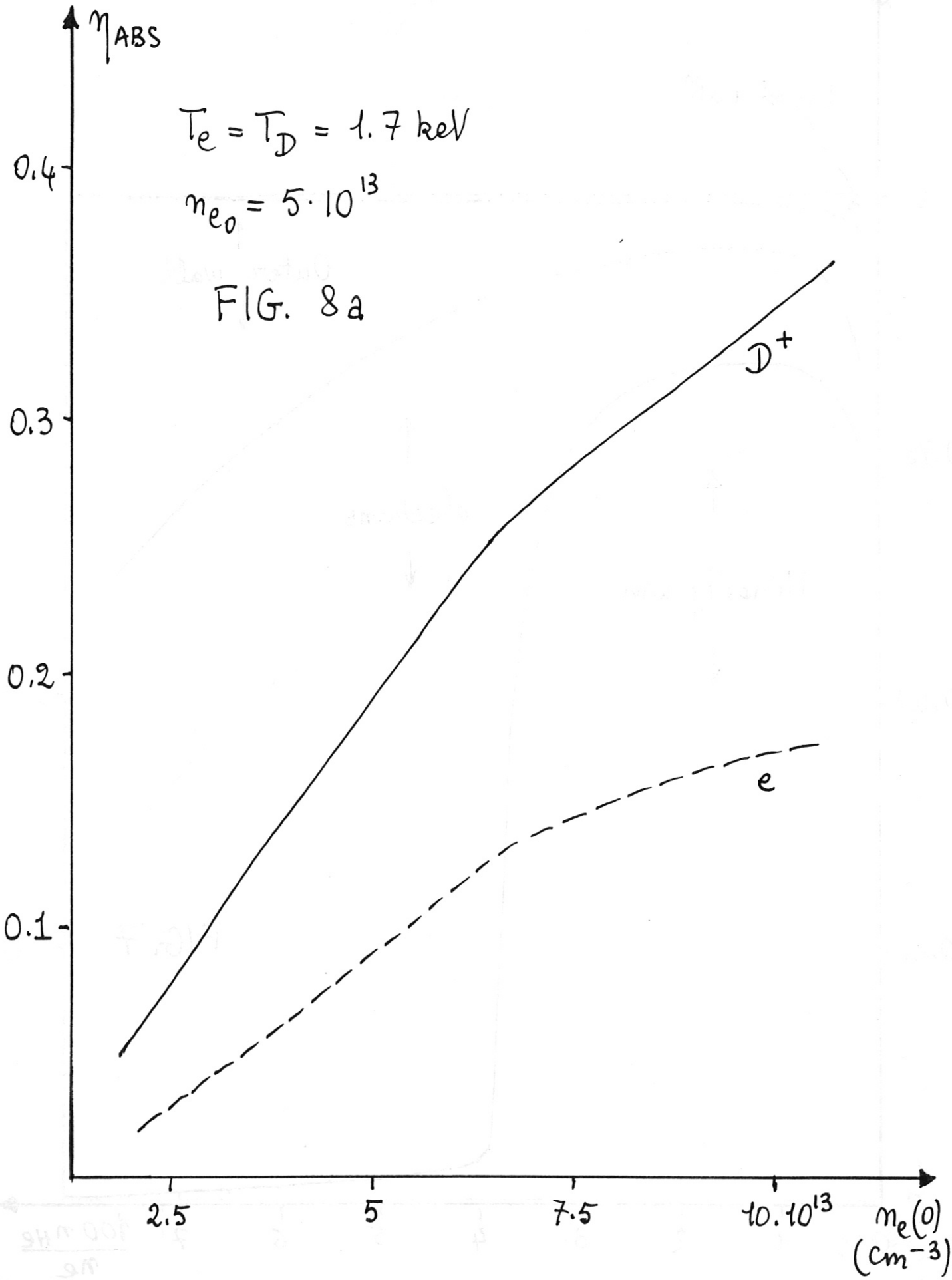
η_{ABS}
$T_e = T_D = 1.7$ keV
$n_{e_0} = 5 \cdot 10^{13}$
0.4
0.3
0.2
0.1
D^+
e^-
2.5
5
7.5
10.10^{13}
$n_e(0)$
(cm^{-3})

FIG. 8a

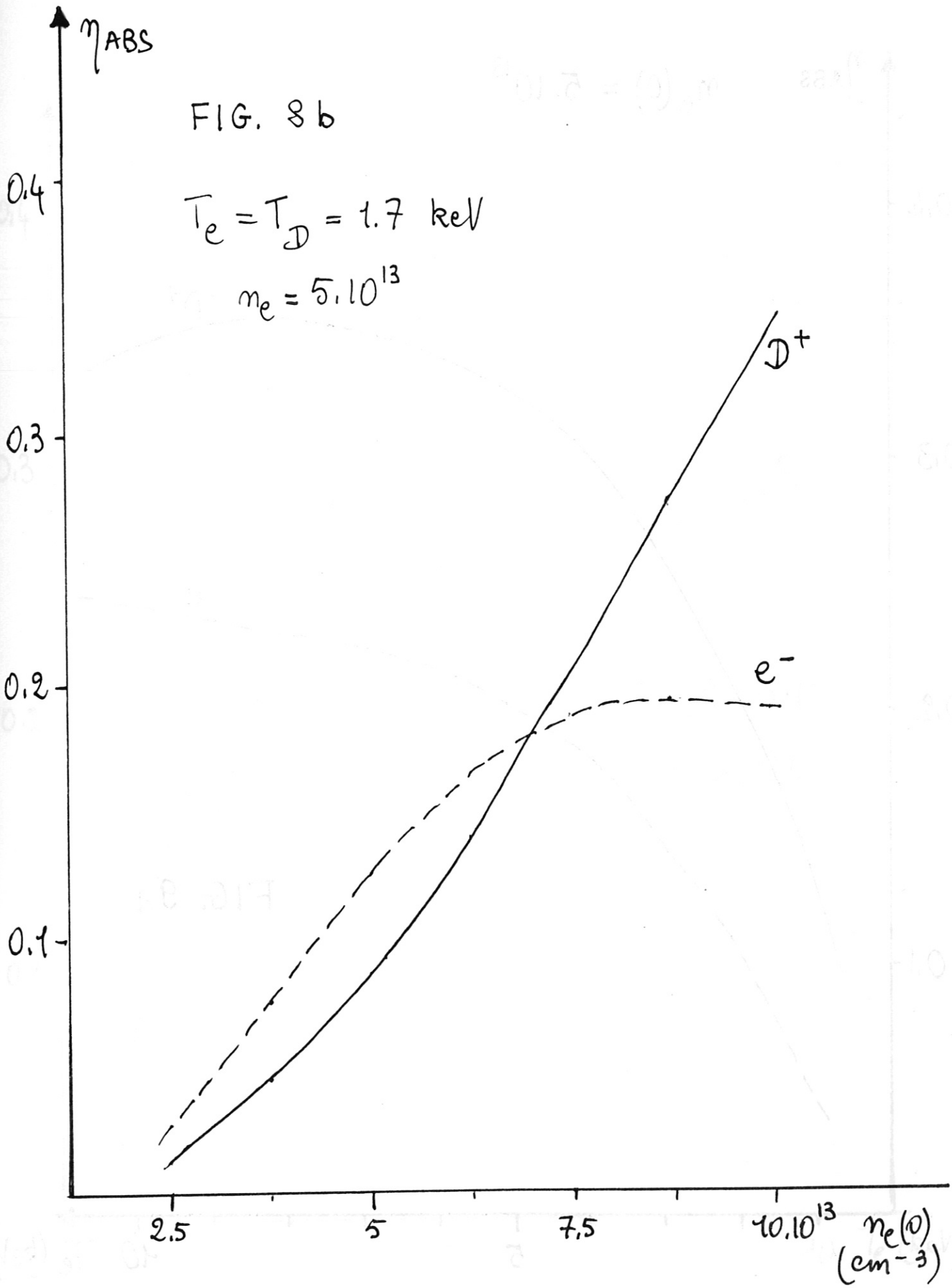
η_{ABS}
FIG. 8b
$T_e = T_D = 1.7$ keV
$n_e = 5.10^{13}$
0.4
0.3
0.2
0.1
D^+
e^-
2.5
5
7.5
10.10^{13}
$n_e(0)$
(cm^{-3})

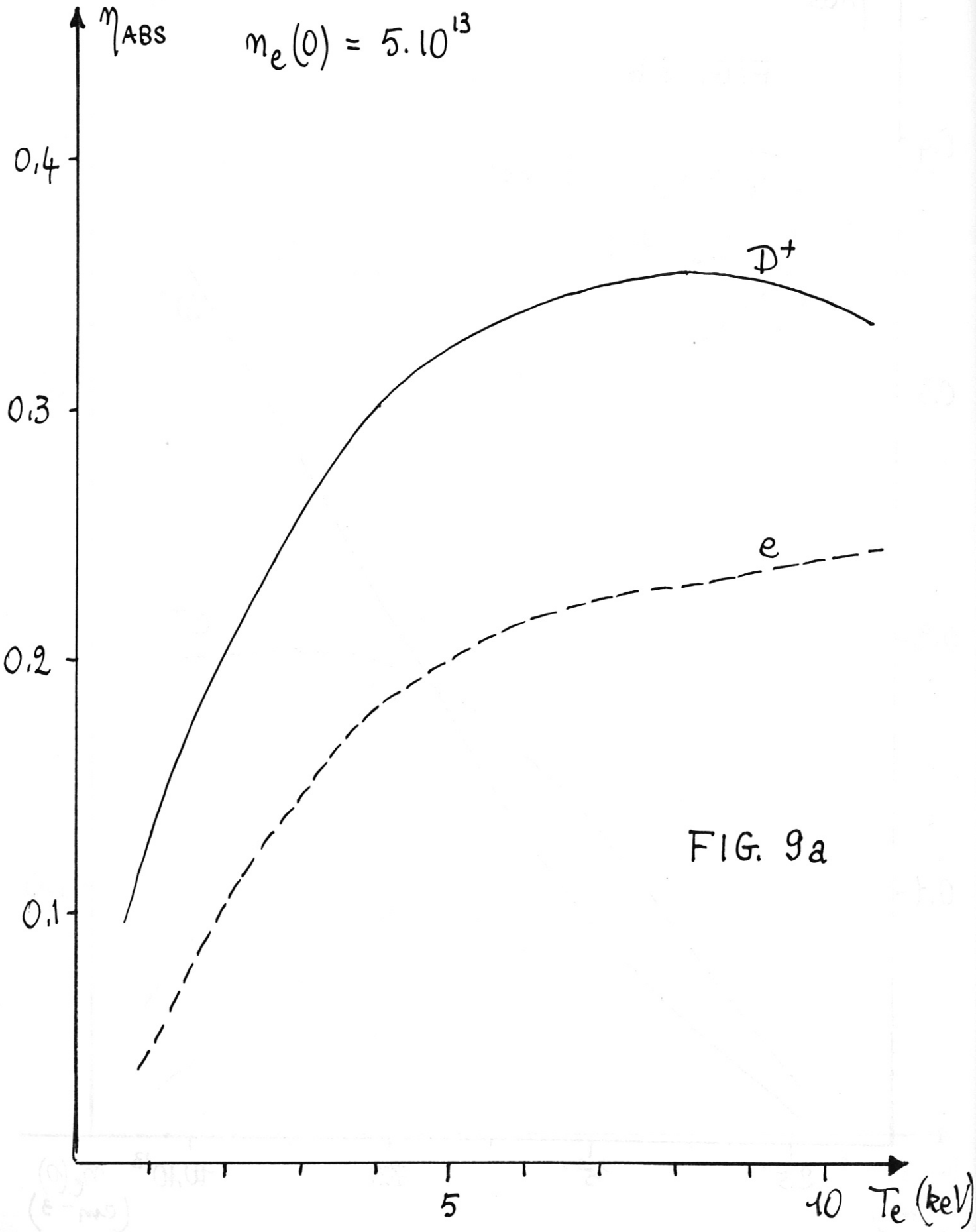

FIG. 9a

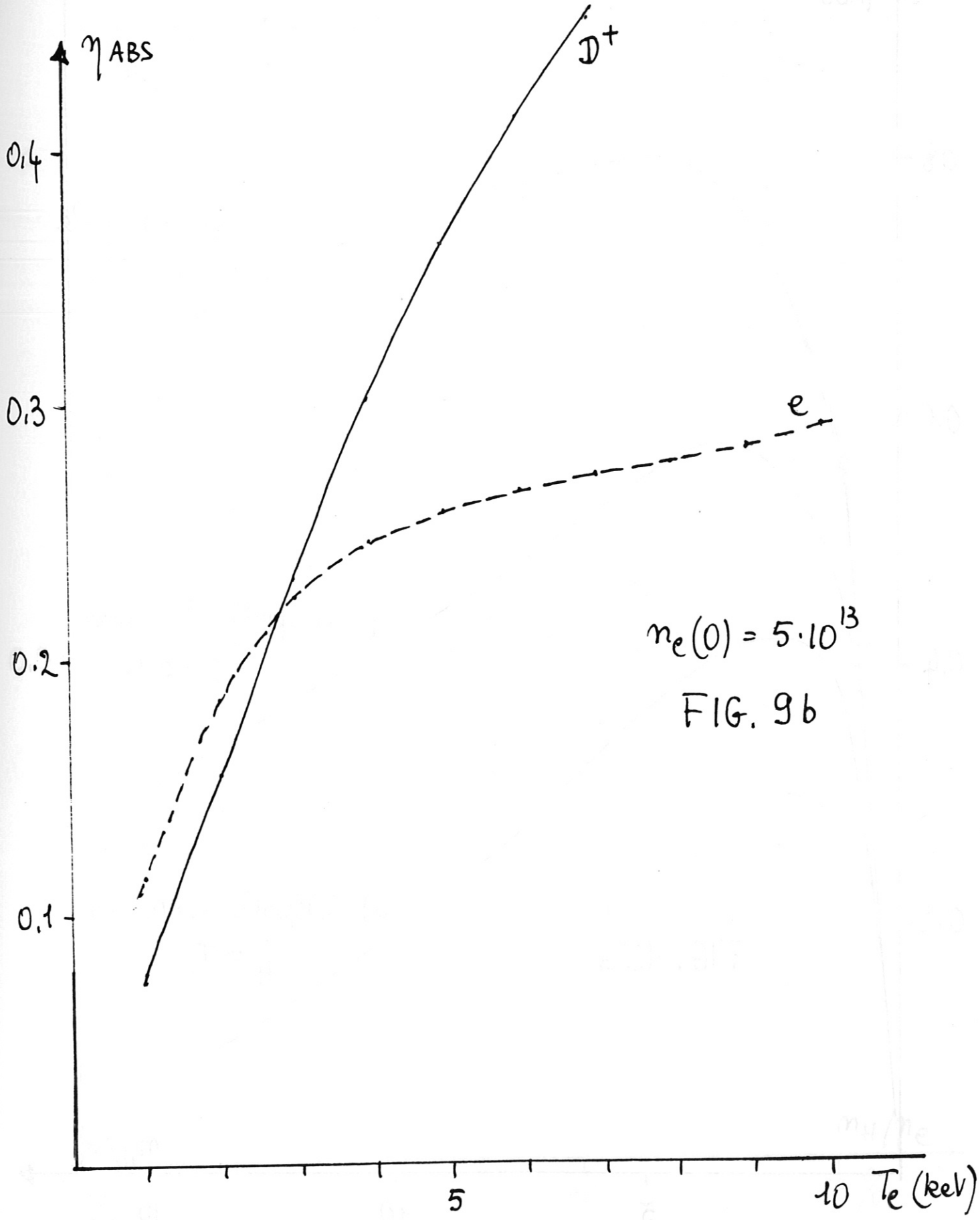

$n_e(0) = 5 \cdot 10^{13}$

FIG. 9b

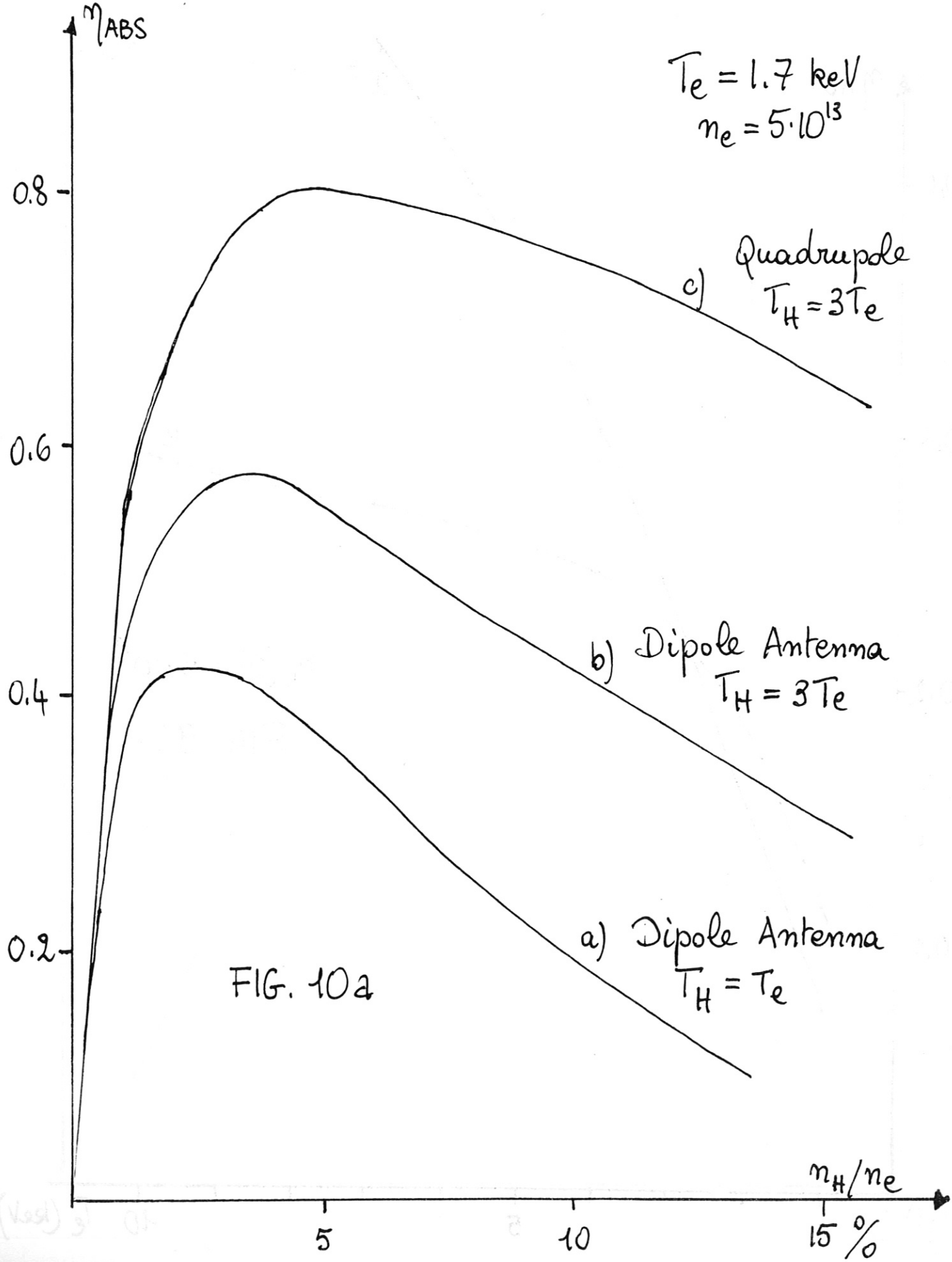
η_{ABS}
$T_e = 1.7$ keV
$n_e = 5 \cdot 10^{13}$
0.8
0.6
0.4
0.2
c) Quadrupole
$T_H = 3T_e$
b) Dipole Antenna
$T_H = 3T_e$
a) Dipole Antenna
$T_H = T_e$
n_H/n_e
5
10
15 %

FIG. 10a

FIG. 10 b

$T_e = 1.7$ keV

$n_e = 5 \cdot 10^{13}$

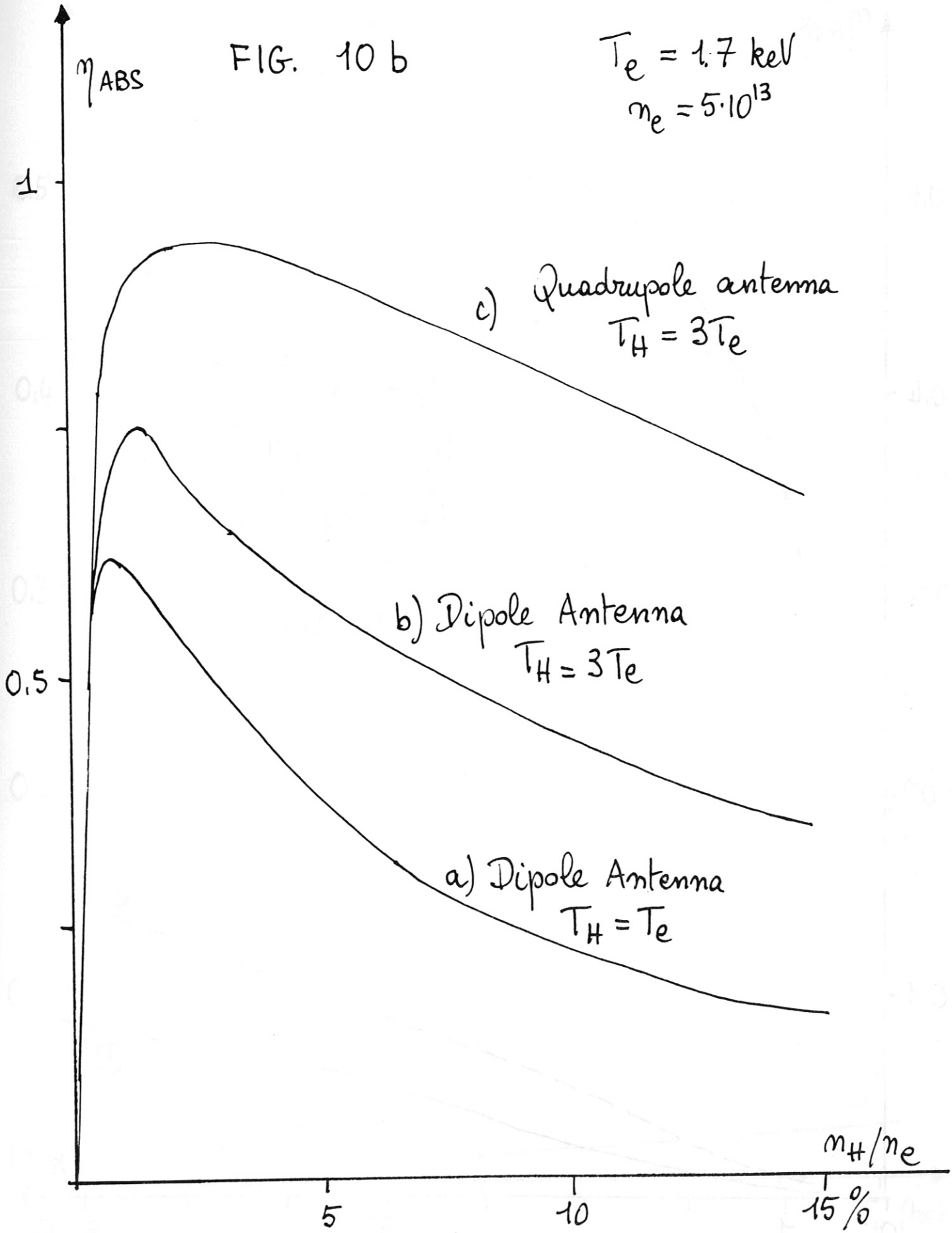

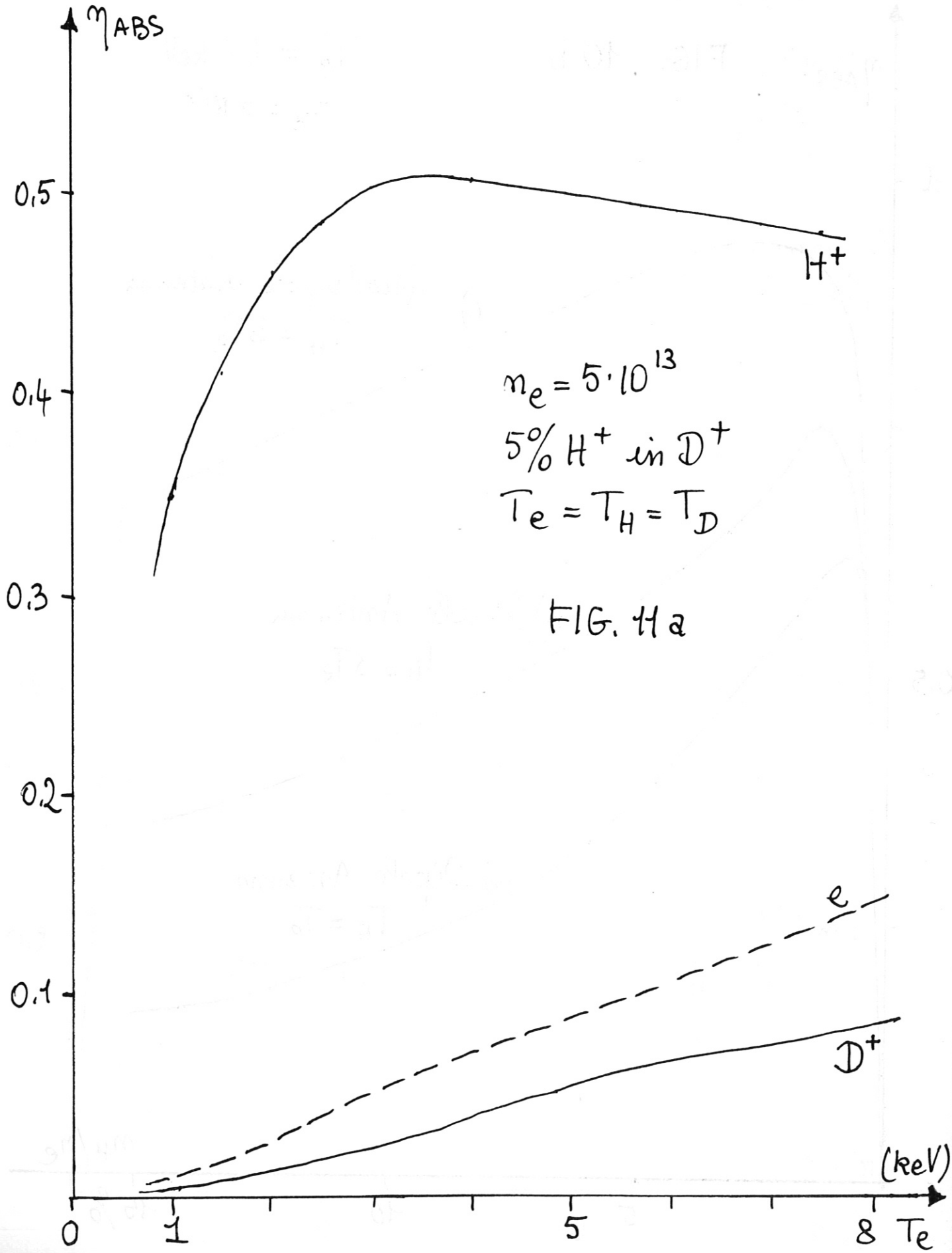
η_{ABS}
0,5
0,4
0,3
0,2
0,1
H^+
$n_e = 5 \cdot 10^{13}$
5% H^+ in D^+
$T_e = T_H = T_D$
e
D^+
(keV)
0
1
5
8
T_e

FIG. 4a

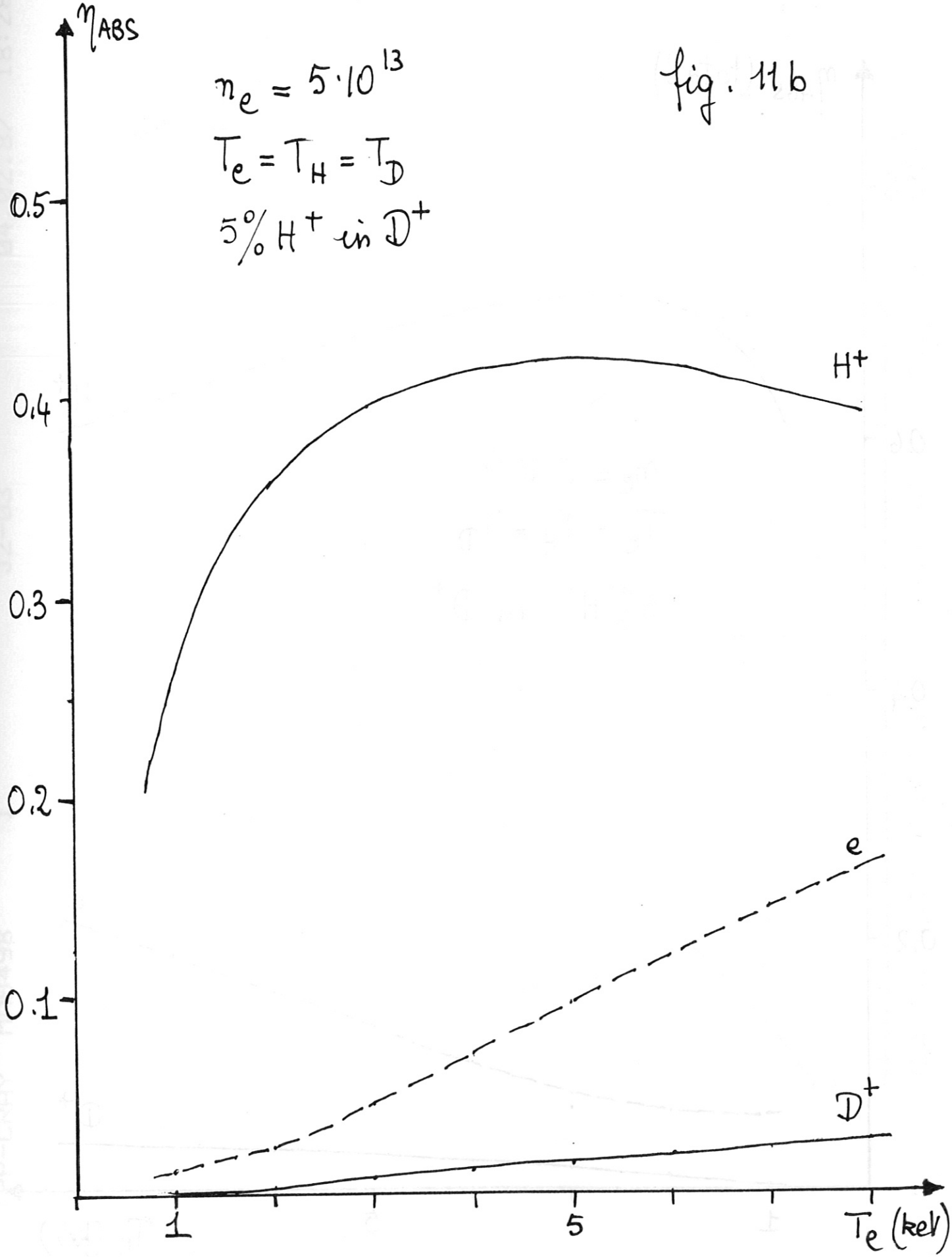
η_{ABS}
$n_e = 5 \cdot 10^{13}$
$T_e = T_H = T_D$
5% H^+ in D^+
fig. 11b
0.5
0.4
0.3
0.2
0.1
H^+
e
D^+
1
5
T_e (kev)

fig. 12

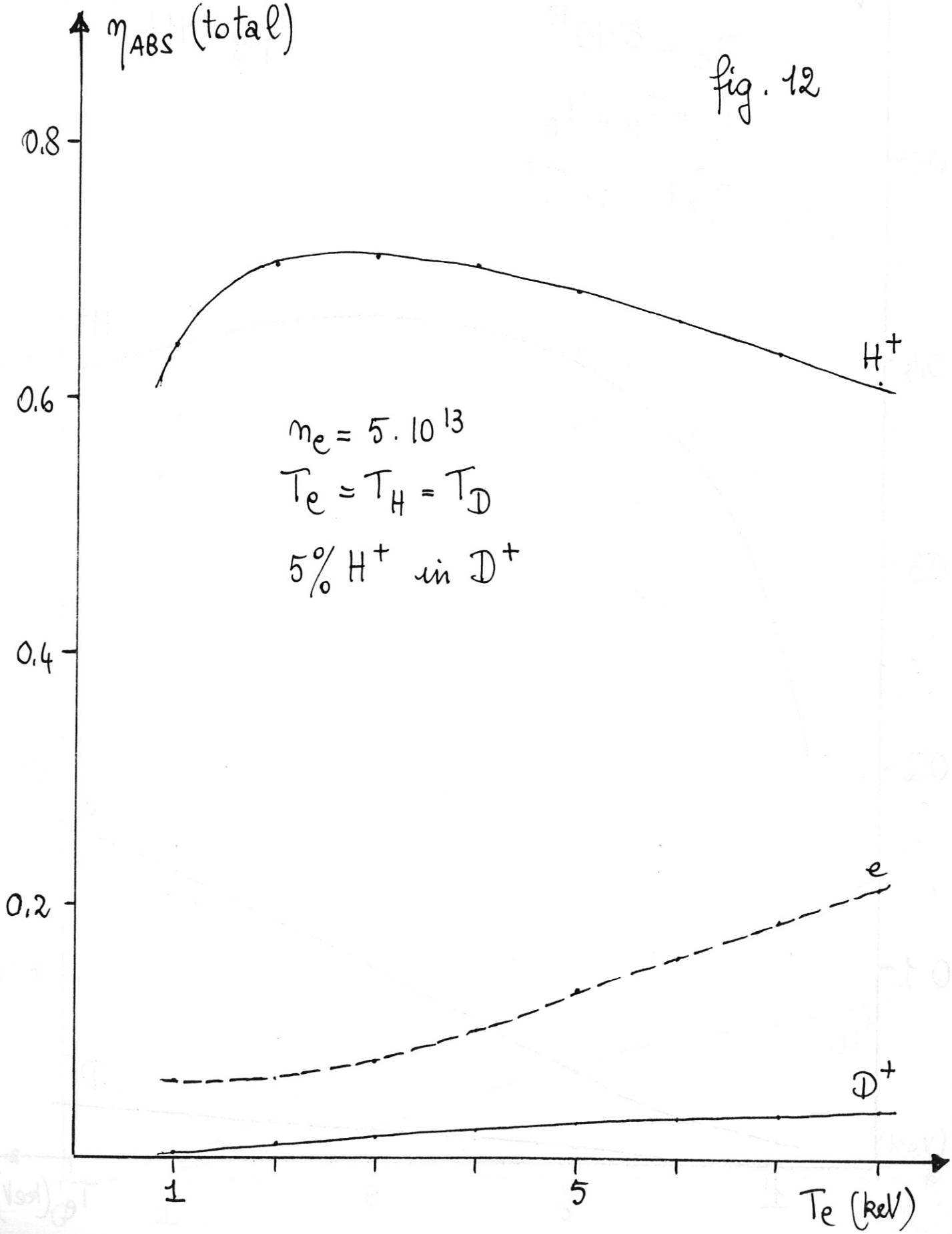
η_{ABS} (total)
0.8
0.6
0.4
0.2
H^+
$n_e = 5.10^{13}$
$T_e \simeq T_H = T_D$
5% H^+ in D^+
e
D^+
1
5
Te (keV)

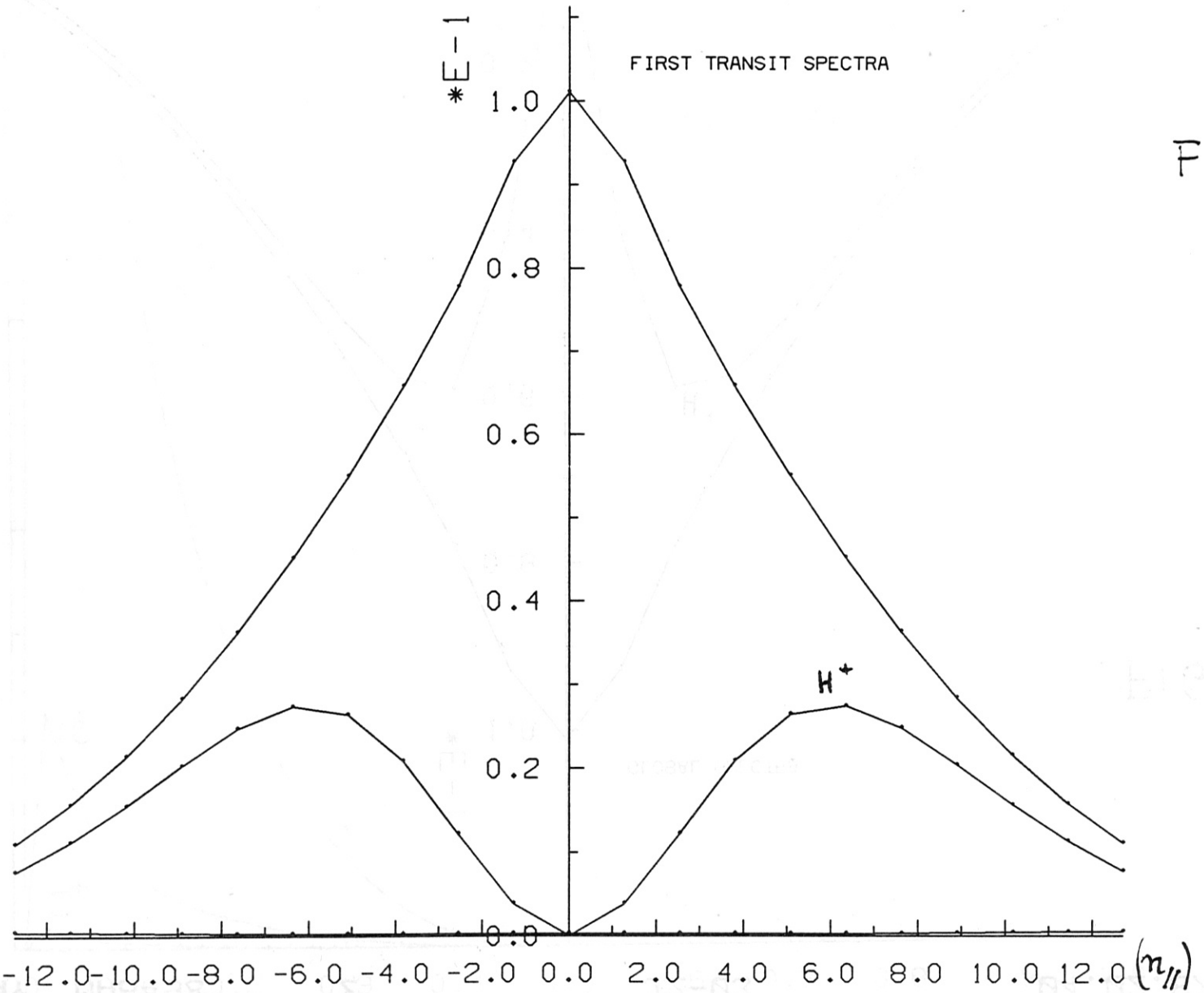
FIRST TRANSIT SPECTRA
*E-1
1.0
0.8
0.6
0.4
0.2
0.0
H+
-12.0 -10.0 -8.0 -6.0 -4.0 -2.0 0.0 2.0 4.0 6.0 8.0 10.0 12.0
(n//)

FIG. 13 a

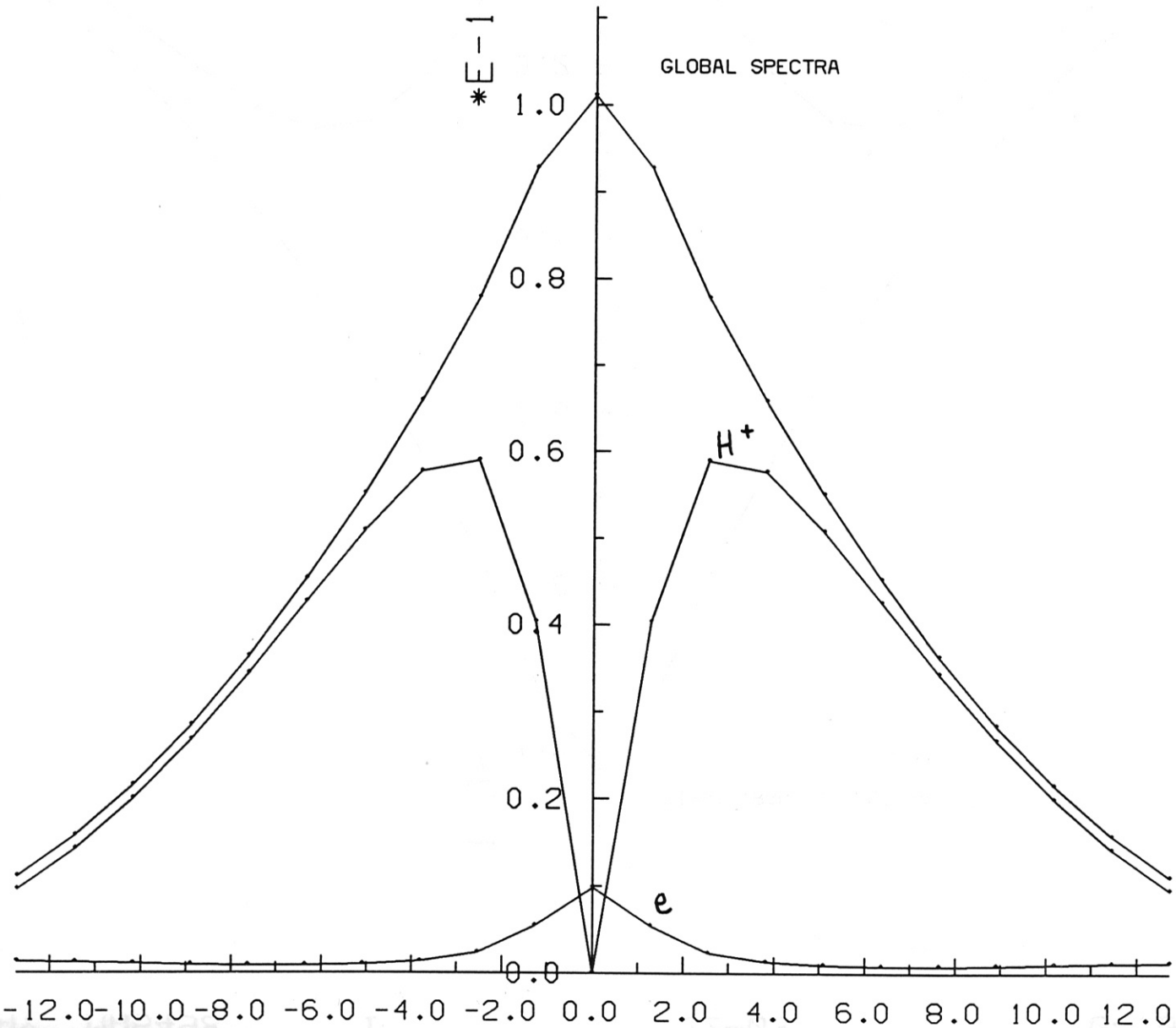
GLOBAL SPECTRA
*E-1
1.0
0.8
0.6
0.4
0.2
0.0
H+
e
-12.0 -10.0 -8.0 -6.0 -4.0 -2.0 0.0 2.0 4.0 6.0 8.0 10.0 12.0
(n_||)

FIG. 13b

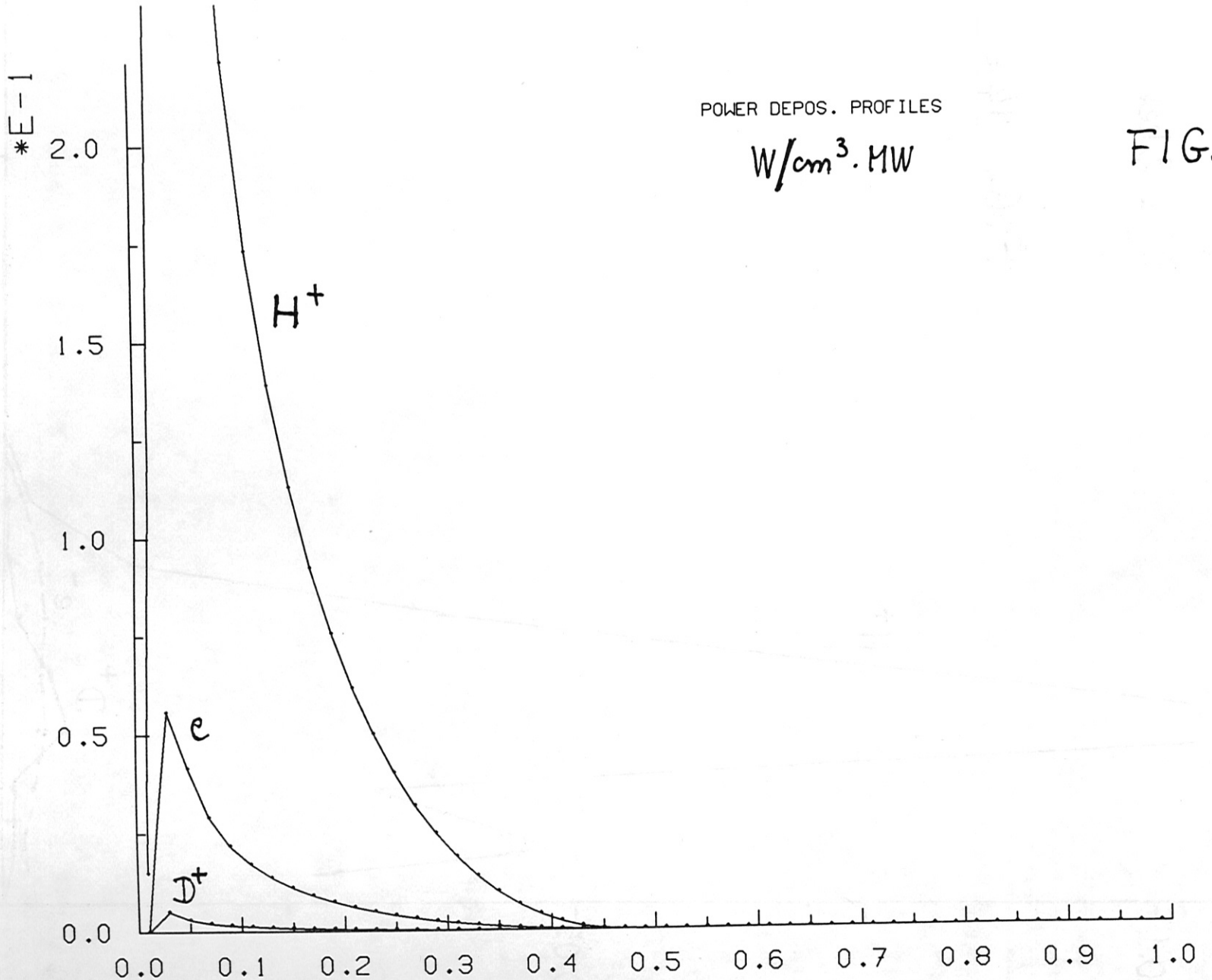

POWER DEPOS. PROFILES

$W/cm^3 . MW$

FIG. 14 a

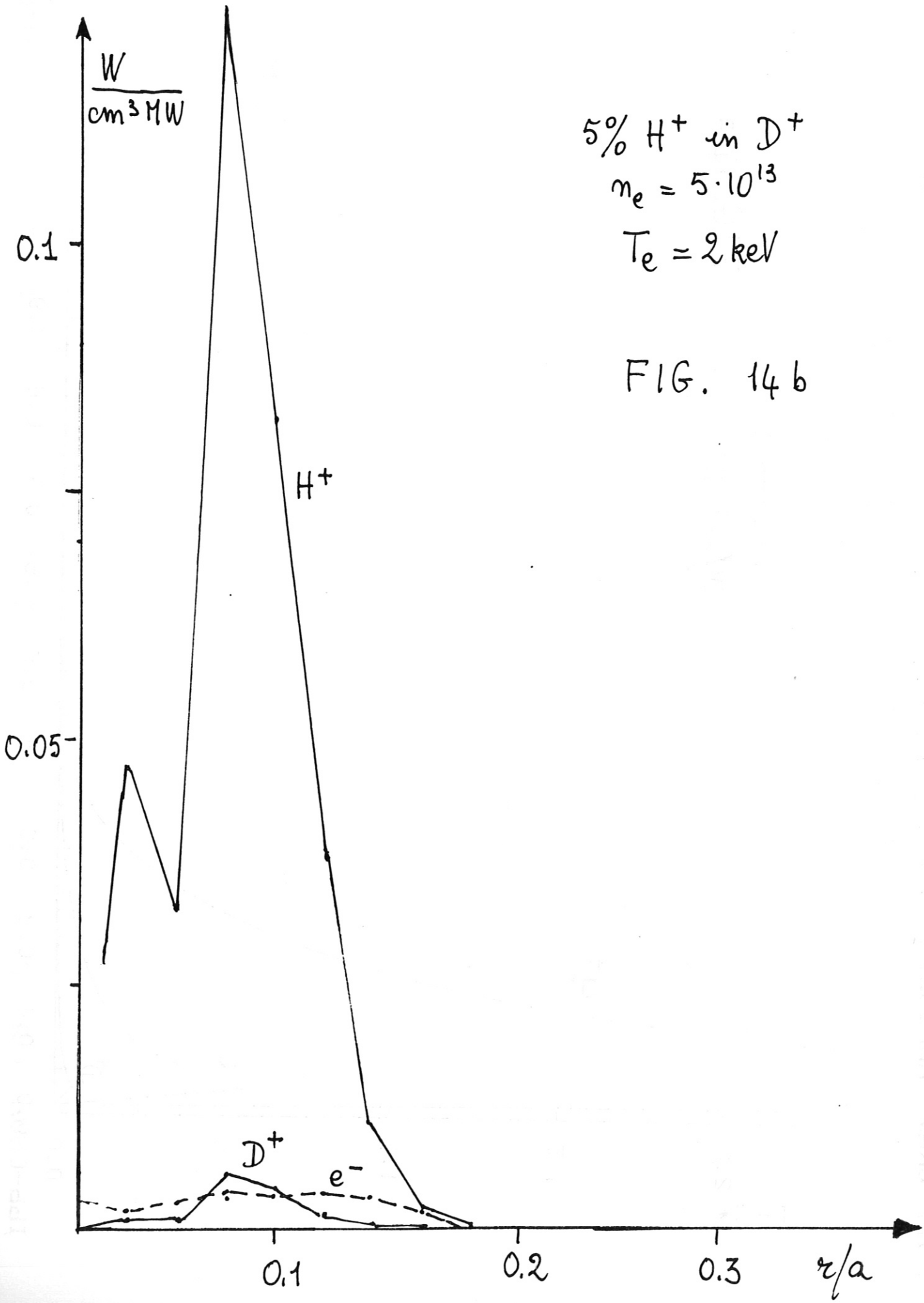

5% H^+ in D^+

$n_e = 5 \cdot 10^{13}$

$T_e = 2$ keV

FIG. 14 b